



JOHN F. KENNEDY SPACE CENTER

TR-145-D
March 8, 1965

ENGINEERING LUNAR MODEL OBSTACLES (ELMO)

by

J. R. Olivier
R. E. Valentine

N65-24717

FACILITY FORM 602

(ACCESSION NUMBER)	(THRU)
<u>56</u>	<u>1</u>
(PAGES)	(CODE)
<u>TMX-56451</u>	<u>30</u>
(NASA CR OR TMX OR AD NUMBER)	(CATEGORY)

GPO PRICE \$ _____

OTS PRICE(S) \$ _____

Hard copy (HC) 3.00

Microfiche (MF) .50

FUTURE STUDIES BRANCH
LAUNCH SUPPORT EQUIPMENT ENGINEERING DIVISION

March 8, 1965

KENNEDY SPACE CENTER

TR-145-D

ENGINEERING LUNAR MODEL OBSTACLES (ELMO)

by

J. R. Olivier
R. E. Valentine

ABSTRACT

This report presents an analytical procedure for determining the energy required by a Lunar roving vehicle for negotiating small obstacles. Some results of a limited parametric analysis generated by the use of this procedure are included. Energy requirements are calculated for a typical vehicle to illustrate the use of the data, and to establish a base line value.

author

524717

24717

March 8, 1965

KENNEDY SPACE CENTER

TR-145-D

ENGINEERING LUNAR MODEL OBSTACLES (ELMO)

by

J. R. Olivier
R. E. Valentine

FUTURE STUDIES BRANCH

LAUNCH SUPPORT EQUIPMENT ENGINEERING DIVISION

TABLE OF CONTENTS

<u>Section</u>	<u>Title</u>	<u>Page</u>
I	INTRODUCTION	
	A. PURPOSE	1-1
	B. DESCRIPTION	1-1
II	ANALYTICAL METHOD	
	A. GENERAL	2-1
	B. ASSUMPTIONS	2-1
	C. OBSTACLE PROFILE DEFINITION	2-2
	D. ENERGY CALCULATION FOR ONE AXLE	2-5
	E. ENERGY CALCULATION FOR MULTI-AXLE VEHICLES	2-9
III	PARAMETRIC ANALYSIS	
	A. APPROACH.....	3-1
	B. DETERMINATION OF n	3-1
	C. PARAMETRIC DATA	3-3
IV	ANALYSIS OF DATA	
	A. GENERAL.....	4-1
	B. DETERMINATION OF ENERGY FOR OBSTACLES	4-1
V	CONCLUSIONS AND RECOMMENDATIONS	
	A. GENERAL	5-1
	B. CONCLUSIONS	5-1
	C. RECOMMENDATIONS	5-1
	APPENDIX	A-1

LIST OF ILLUSTRATIONS

<u>Number</u>	<u>Title</u>	<u>Page</u>
2-1.	Roughness Profiles for Various Values of C	2-3
2-2.	Mathematics of Energy Calculation	2-7
2-3.	Energy Determination Procedure for One-Axle Vehicle	2-8
2-4.	Energy Determination Procedure for Two-Axle Vehicles	2-10
3-1.	Energy Versus Energy Summing Interval	3-2
3-2.	2σ Variation for Various Distances Traveled	3-4
3-3.	Energy Versus C for Various Wheel Diameters (Two Axles)	3-5
3-4.	Energy Versus C for Various Wheel Diameters (Three Axles)	3-6
3-5.	E Versus C for Various Values of DI	3-8
3-6.	E Versus Y_{\max} for Various Values of D	3-9
3-7.	E Versus D for Various Values of Y_{\max}	3-10
3-8.	E Versus Number of Axles for Various Values of D	3-11
3-9.	Energy Variation with Weight Distribution for Two and Three Axles	3-13
4-1.	Percent of Mobility Energy for Obstacle Negotiation Versus C From Sample Problem	4-2

DEFINITION OF SYMBOLS

SYMBOL	DEFINITION
C	Obstacle distribution exponent
D	Wheel diameter, cm
DI	Obstacle definition interval, cm
DX	Energy summation interval, cm
E	Normalized mobility energy, kw-hr per km per 1000 kg
E'	Total energy to traverse distance S, kw-hr
$\Delta E'$	Change in energy between two adjacent points in the summation, kw-hr
H	Wheel center height above the X-axis, cm
(k, h)	Coordinates of the center of a circle
m	Vehicle total mass, kg
m_1	Mass on first axle, kg
m_2	Mass on second axle, kg
n	Energy summation limit
NW	Number of axles
R_1	Percentage of mass on first wheel, kg
R_2	Percentage of $(m - m_1)$ on second wheel
RN	Random number
S	Distance over which energy is calculated, km
WB	Wheelbase, cm

DEFINITION OF SYMBOLS (Cont.)

SYMBOL	DEFINITION
WS	Wheel separation, cm
(X, Y)	Coordinates of a point on the circumference of a circle
Y	Obstacle height, cm
Y_{\max}	Maximum obstacle height, cm

SECTION I INTRODUCTION

A. PURPOSE

The purpose of this report is to present the results of an analytical study of Lunar roving vehicle energy requirements for negotiating small obstacles.

B. DESCRIPTION

A large study effort is underway that will result in the preliminary design of a Lunar roving vehicle. A study of such magnitude requires investigation in many areas. The area of interest in this report is that of vehicle mobility, and, more specifically, the energy required for mobility purposes.

Vehicles traveling across the Lunar surface will require mobility energy for ascending slopes, overcoming resistance due to sinkage in soft soils, and for going over obstacles too small to require circumnavigation. Much work has been done towards describing the characteristics of the Lunar surface from available photographic data. The results of such an analysis are reported in TR-83-D¹ in the form of frequency of slope occurrence over representative paths. The analysis was taken one step further by assigning soil characteristics to the various slopes. With such complete data, it is possible to compute the energy required for a vehicle to traverse such a terrain. The only factor missing is the energy required to negotiate obstacles so small as to make it impractical to circumnavigate them.

The problem was recognized in the work discussed above but no attempt was made to find a solution. Instead, a recommendation was made that an energy reserve of 20 percent be included to cover small obstacle negotiation. This 20 percent has been used in all analytical work with no effort being made to either substantiate or disprove it.

Such a gross estimation is sufficient for very preliminary work but, at some point, must be substantiated. Since no analytical method could be found for defining the micro-profile of the Lunar surface and for computing energy required for traversing such a profile, the method presented here was developed to fill the need.

¹"Engineering Lunar Model Surface (ELMS)", September 4, 1964, Kennedy Space Center, NASA.

The procedure uses two parameters, terrain definition spacing and terrain elevation, to describe surface roughness. Terrain definition spacing is used as a specified constant value. Elevations are chosen randomly according to a particular distribution function. A surface profile reproduced from such a system yields a series of discrete points.

This method, based on sound concepts, is a good approach for the initial attempt at determining energy requirements for traversing the micro-profile of the Lunar surface. It is recognized that, as Lunar surface data becomes available, it may be necessary to alter the profile description to more closely approximate the actual surface. The use of points for surface description, as compared to lines, will be of major interest.

If the surface is undulating, as indicated by available photographic data it could be necessary to employ a profile description system using lines rather than points.

SECTION II ANALYTICAL METHOD

A. GENERAL

It is very difficult to define roughness for the Lunar surface; however, it is a necessary step in estimating the required energy values for mobility. The term "obstacles" is used to refer to terrain features with elevations less than about two and one-half times the wheel diameter.

The analytical method requires two steps;

Step 1 - Establish an obstacle profile.

Step 2 - Compute energy as the vehicle is moved across this profile.

B. ASSUMPTIONS

The following assumptions were used in the analytical procedure to be described.

- (1) The reference plane is horizontal.

This simply means that energy values shown do not include energy required for ascending slopes.

- (2) Vehicle mass acts at the wheel center.

No shift of mass is considered due to center of gravity height. The error introduced will be shown to be negligible.

- (3) The vehicle moves in only two dimensions.

Wheels on only one side of a vehicle are considered so that number of wheels in this analysis is actually number of axles for a three-dimensional vehicle.

- (4) Wheels are rigid.

The effects of flexible wheels are not considered.

- (5) Energy values are ideal energies.

No attempt has been made to take into account inefficiencies such as wheel slip, drive train energy loss, etc.

- (6) Wheel spacing is assumed to be constant.

As wheels move vertically in a multi-wheel vehicle, the wheel spacing changes. So, wheel base is actually the distance between wheel centers only when the wheels are on the same level. A side investigation indicated that even large changes in wheel base had negligible effect so the error introduced by this assumption is very small.

- (7) Inertia effects are not considered.

No account is taken of the effect of the dynamics of the moving vehicle.

C. OBSTACLE PROFILE DEFINITION

Roughness of the Lunar surface is defined by specifying a spacing between obstacles and an obstacle height. Spacing can be random or can be a specified constant value. This procedure uses a constant spacing since this method is used when measurements are actually made in situ. Obstacle height is chosen by a random process wherein a maximum height, Y_{\max} , is specified and the obstacle heights varied from zero to Y_{\max} based on the following arbitrarily chosen distribution function:

$$Y = Y_{\max} (RN)^C \quad (1)$$

Where RN is a random number

Figure 2-1 depicts how an obstacle profile will appear for various values of the distribution exponent, C . For the cases shown, the spacing interval, DI , is 20 cm and Y_{\max} equals 50cm. A C value of one gives a completely random surface with equal numbers of obstacles in each obstacle height range. Going to a C less than one changes the distribution so that the mean obstacle height approaches Y_{\max} . As C increases above one, the distribution changes so that the mean obstacle height becomes less and less. The profiles in figure 2-1 seem to indicate that the surface is very smooth for large values of C . This is due to the fact that only a very short distance is shown. The frequency values have been given to aid in evaluating roughness. The lower number indicates the

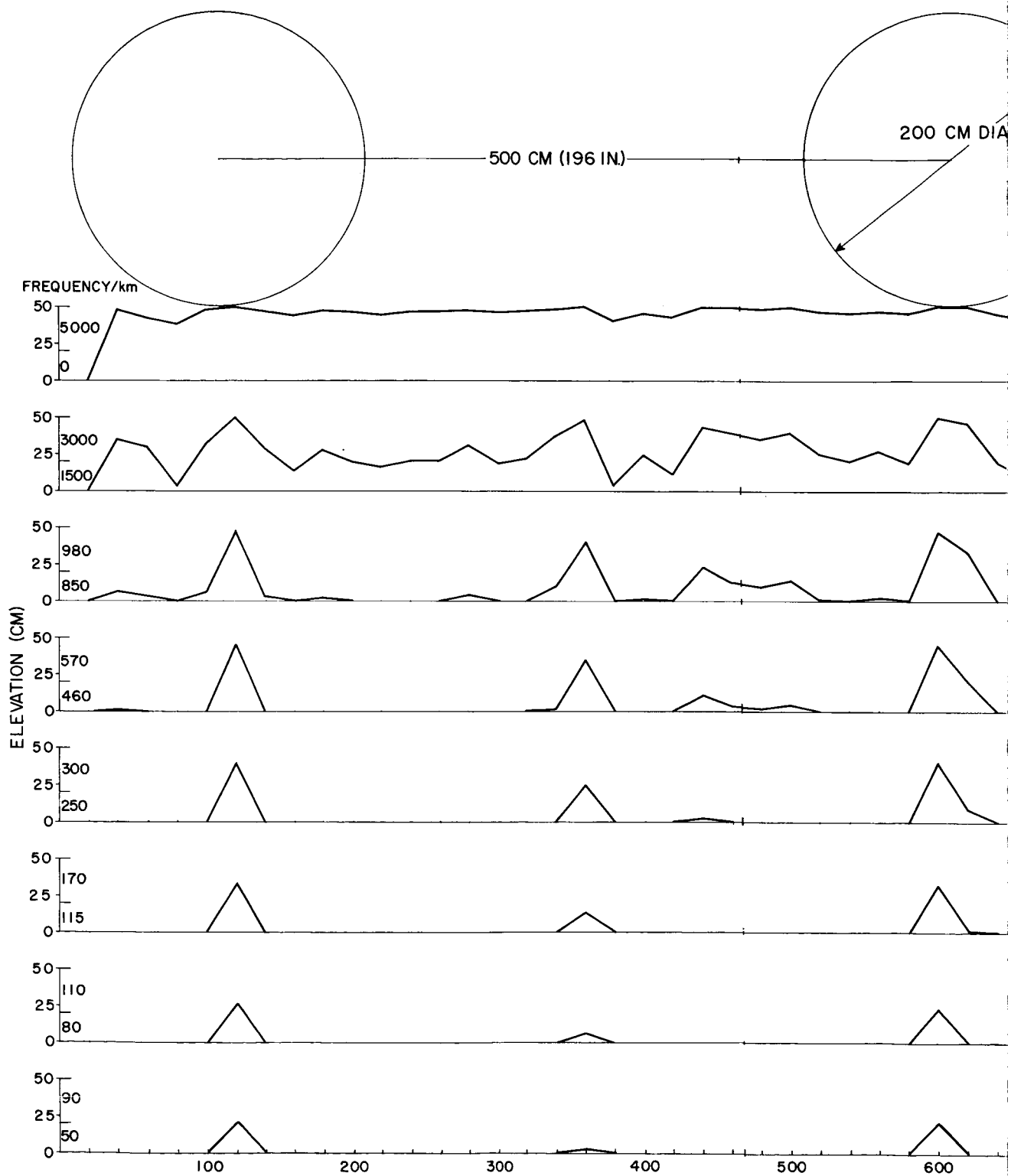
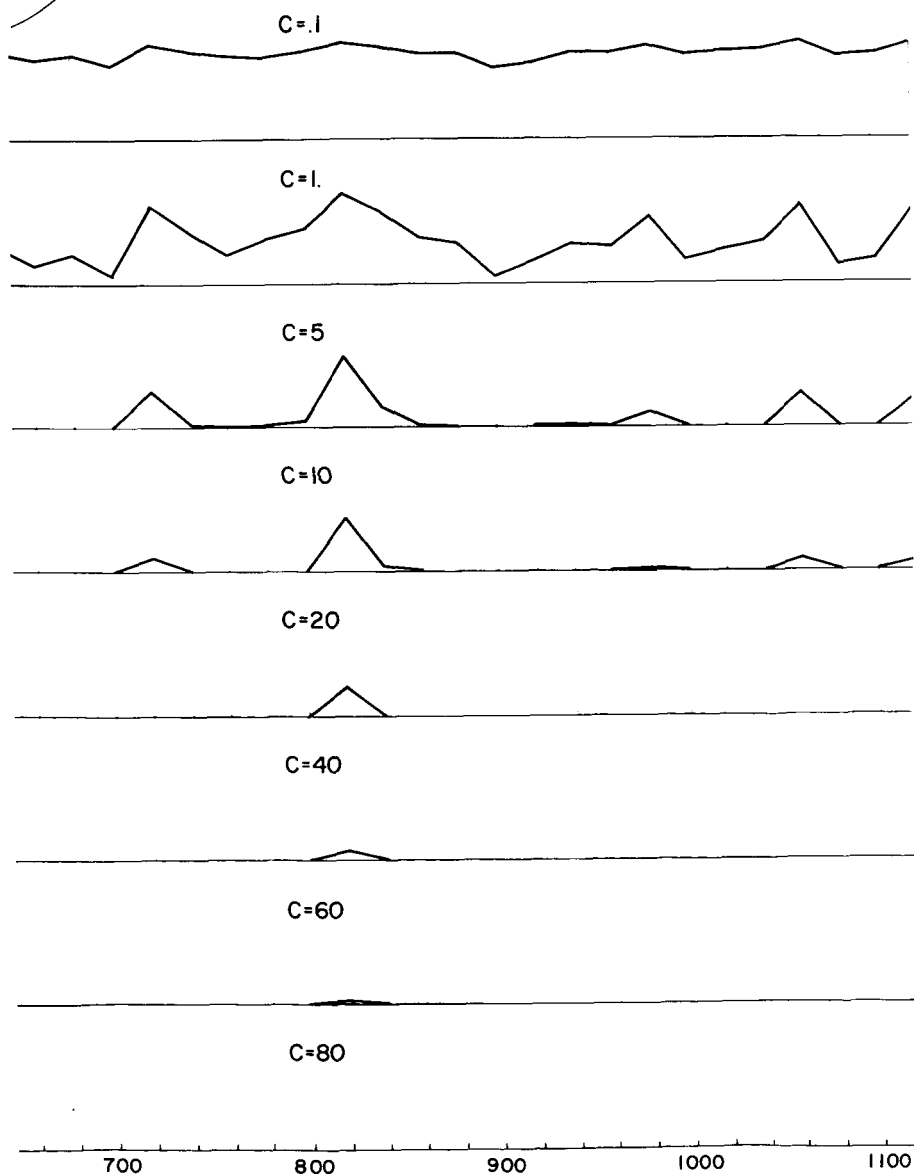
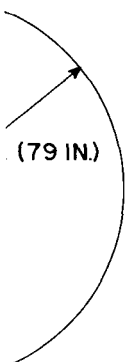


Figure 2-1. Roughness Profiles for Various Values of C

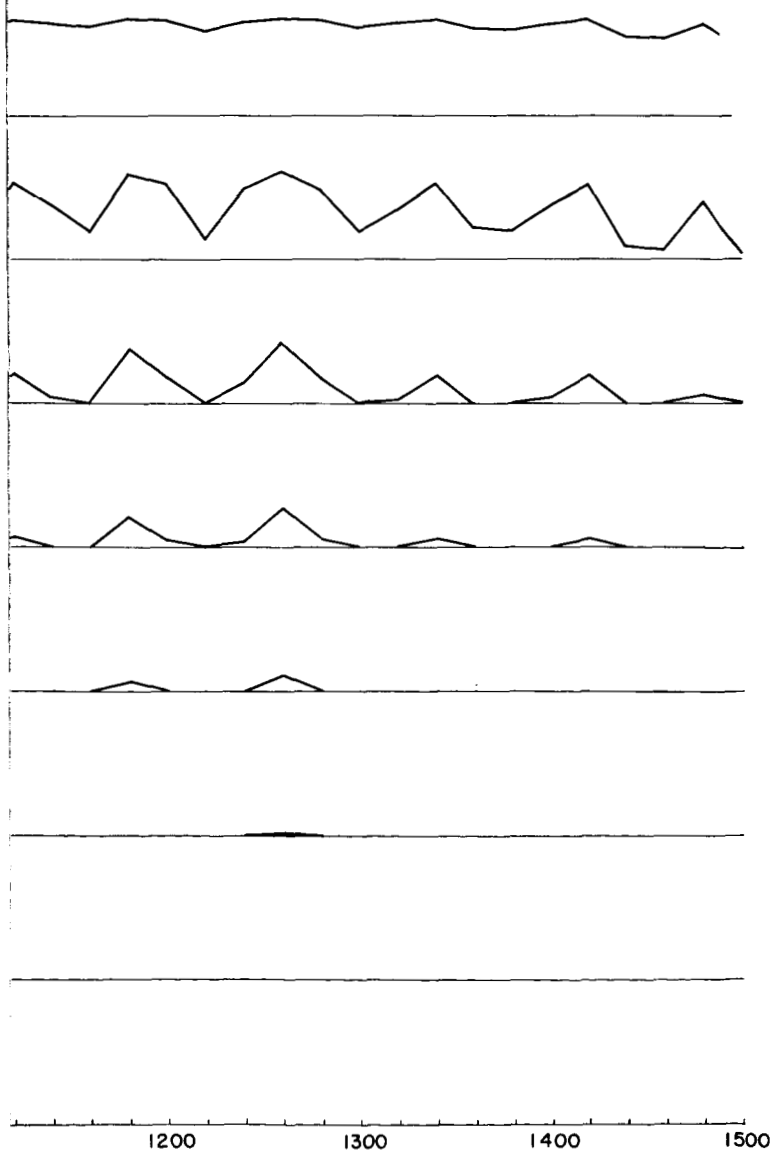
PROFILE CLASSIFICATION

$$(Y = Y_{\text{MAX}} \times R N^C)$$



DISTANCE (CM)

B



C

number of obstacles per kilometer with heights between 5 and 20 cm while the upper value shows the number of obstacles with heights between 20 and 50 cm per kilometer. If the frequency value is multiplied by the total number of kilometers to be traversed, it becomes apparent that even for C of 80 a very large number of obstacles must be negotiated.

D. ENERGY CALCULATION FOR ONE AXLE

The energy calculation is begun by defining an obstacle profile using the method described above. A vehicle is placed on the path and its potential energy, referenced to some datum plane, is calculated. The vehicle is moved horizontally some distance, DX, and its potential energy calculated again. If the energy increases, the difference is retained. If the energy decreases, the change is ignored. This is continued over the entire path to yield an energy requirement that is equal to the sum of the potential energy increases. Potential energy decreases are ignored because the vehicle layout precludes any coasting.

Reference is made to figure 2-2 during the following discussion of the mathematics of energy calculation. One wheel is shown crossing an obstacle profile with an exaggerated spacing of DI. The procedure is started with the wheel located in position I. The Y' axis will be shifted so that it always passes through the wheel center. The wheel is moved vertically so that it is tangent to the highest obstacle within the range of the wheel diameter, D. The dashed circular arcs represent different wheel positions as the wheel moves along the Y' axis. Note that the obstacle is only a point and that the connecting lines shown have no consequence. Mathematically, this procedure requires that the coordinates of each obstacle concerned be used in the equation of the circle to determine the H_n for the wheel when it reaches the desired position.

The general equation for any circle is:

$$r^2 = (Y-h)^2 + (X-k)^2 \quad (2)$$

where:

r is the radius

(X, Y) the coordinates of a point on the circle

(k, h) the coordinates of the center of the circle

Since the center of the wheel will always be on the Y' axis, k equals zero; also h equals H_n , so that the equation for the wheel becomes:

$$r^2 = (Y' - H_n)^2 + (X - 0)^2 \quad (3)$$

$$r^2 - X^2 = (Y' - H_n)^2$$

Solving for H_n and setting $r = \frac{D}{2}$ gives:

$$H_n = Y' - \sqrt{\frac{D^2}{4} - X^2} \quad (4)$$

The X and Y' coordinates of each obstacle underneath the wheel are used to compute H values. The wheel is now moved vertically so that the Y' coordinate of the center is the maximum H, or H_n . No energy change is involved since the wheel is assumed to be in this position initially.

The center of the wheel is shifted horizontally by some increment, DX, and the above procedure repeated. If H_{n+1} is greater than H_n , the potential energy change is calculated by:

$$\Delta E' = m (H_{n+1} - H_n) \quad (5)$$

For cases where the wheel moves down the energy would be:

$$E' = 0 \quad (6)$$

If this procedure is continued over the total distance, S, the energy would be:

$$\text{For } H_{n+1} > H_n$$

$$E' = m \left[\sum_{n=0}^n (H_{n+1} - H_n) \right] \quad (7)$$

$$\text{For } H_{n+1} \leq H_n$$

$$E' = 0 \quad (8)$$

$$\text{where } n = \frac{S}{DX}$$

Figure 2-2 was purposely exaggerated to illustrate the shift in the coordinate system. Figure 2-3 gives a more realistic picture of the actual situation. The DI is small compared to D so that several obstacles are defined underneath the

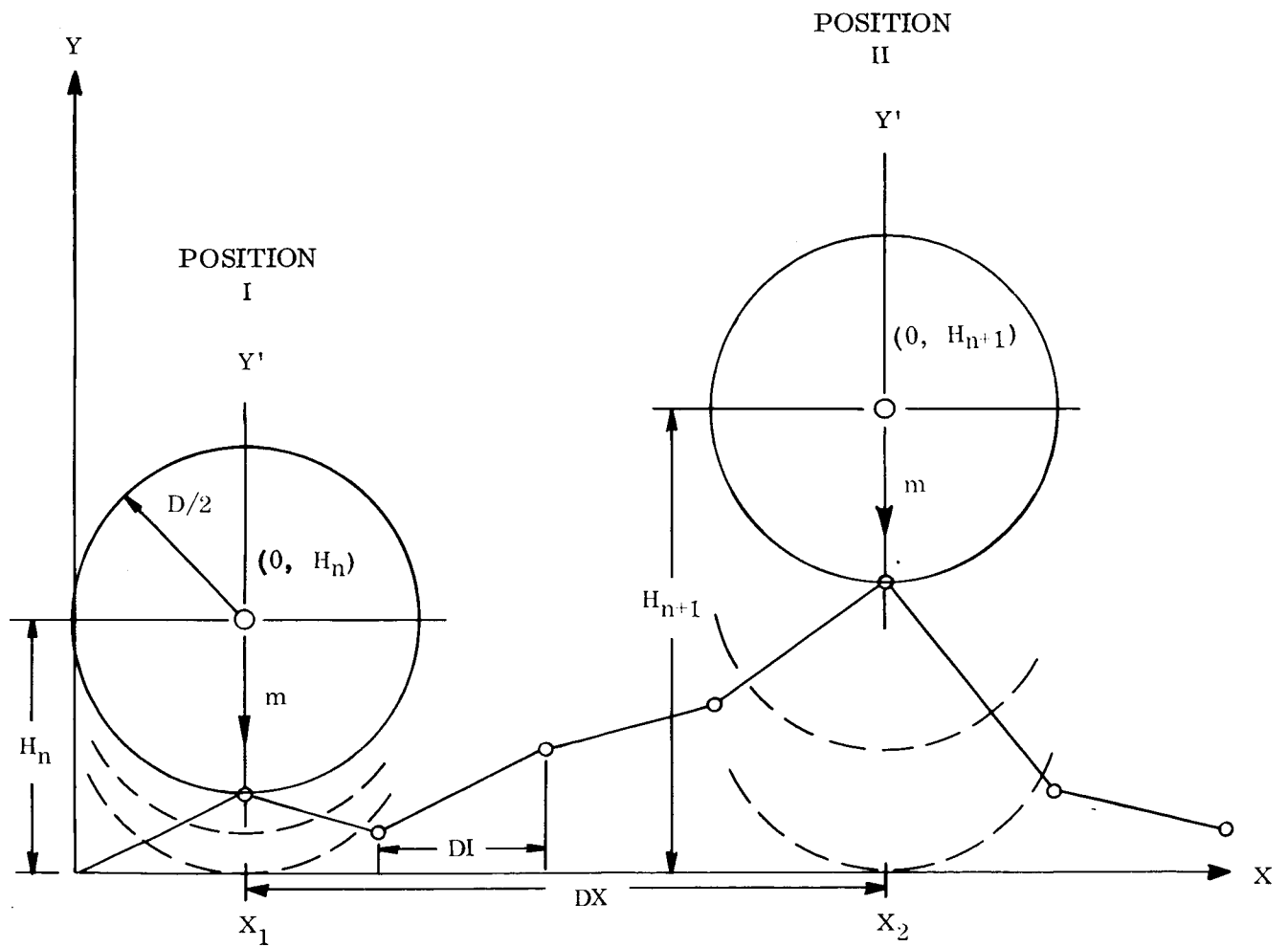


Figure 2-2. Mathematics of Energy Calculation

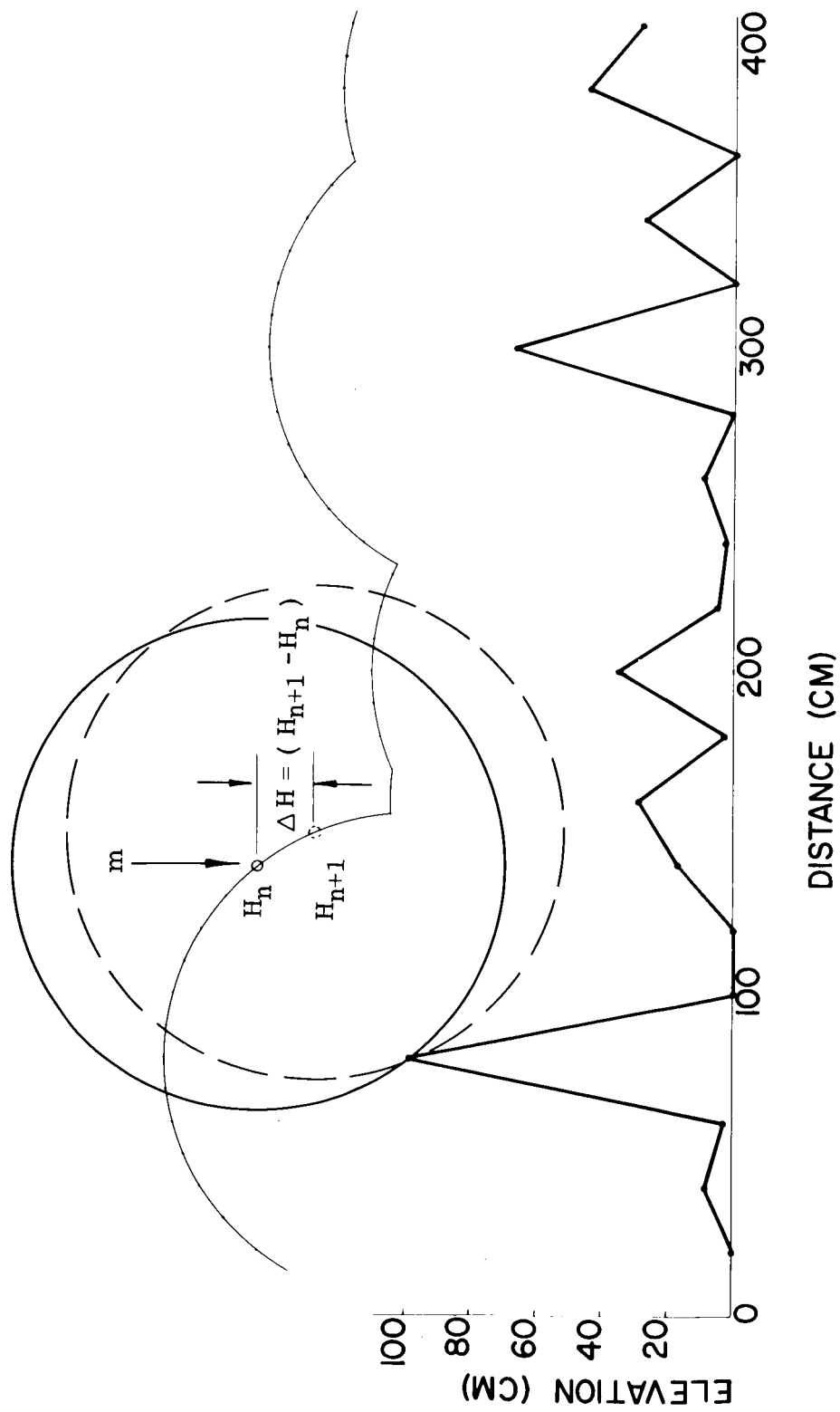


Figure 2-3. Energy Determination Procedure for One -Axle Vehicle

wheel. Also, the DX used is much smaller than shown in figure 2-2. As DX approaches zero, the locus of the wheel center approaches the curved line shown. It is apparent that the accuracy of the summation process is dependent upon the magnitude of DX.

E. ENERGY CALCULATION FOR MULTI-AXLE VEHICLES

Only one axle was considered above; however, the procedure is easily expanded to include any number of axles, NW. Figure 2-4 shows a two-axle vehicle with the wheel centers separated by some fixed value, WB. This WB or wheel base is given by:

$$WB = (NW - 1) (D + WS) \quad (9)$$

where WS is wheel separation

Wheel base enters into energy calculations implicitly. Its only effect is to fix the relative positions between the wheels on the obstacle path. The energy is determined by calculating total vehicle potential; moving the vehicle a DX distance; calculating new energy; and, finding the potential energy change. If, as in the case for one axle, the positive potential energy changes are summed over the entire path, the desired energy is known.

Before the summation equation for multi-axle vehicles can be written, it is necessary to redefine the Y' coordinate of the wheel center. The format $H_{NW,n}$ will be used. For example, $H_{1,1}$ would be the height of the first wheel center in the first position. Using this format for H, the energy summation equation for a two-axle vehicle becomes:

$$E = \sum_{n=0}^n \left[(H_{1,n+1} m_1 + H_{2,n+1} m_2) - (H_{2,n} m_1 + H_{2,n} m_2) \right] \quad (10)$$

Expanding this to include NW axles gives:

$$E = \sum_{n=0}^n \left[(H_{1,n+1} m_1 + H_{2,n+1} m_2 \dots H_{NW,n+1} m_{NW}) - (H_{1,n} m_1 + H_{2,n} m_2 \dots H_{NW,n} m_{NW}) \right] \quad (11)$$

Figure 2-4. Energy Determination Procedure for Two -Axle Vehicles

or simplifying:

$$E = \sum_{n=0}^{\infty} \left[\sum_{j=1}^{NW} (H_{j,n+1} m_j) - \sum_{j=1}^{NW} (H_{j,n} m_j) \right] \quad (12)$$

A computer program for solving equation (12) was written so that a value of n large enough to give reasonably accurate energies could be used. The remainder of this report presents the results of a parametric analysis using this program, plus some interpretation of the data.

SECTION III PARAMETRIC ANALYSIS

A. APPROACH

Since so little is known about the Lunar surface, it is impossible to choose unique values for each variable and use equation (12) to determine energy. The best approach is to generate parametric data centered around the expected values of maximum obstacle height, obstacle separation, etc. A similar approach is necessary for vehicle characteristics since the vehicle design is still fluid.

B. DETERMINATION OF n

The first step is to choose a value for n . This parameter is necessary for the analysis, but of no interest in the results and was not used parametrically. As stated before, the relation for n is:

$$n = \frac{S}{DX} \quad (13)$$

It is simply the number of times energy is calculated and summed for a given distance traveled. Computation time is directly proportional to n which makes it desirable to keep the value as small as is commensurate with sufficient accuracy.

As shown before, DX controls the accuracy of the summation process over a fixed path. A typical vehicle was run over a large distance using DX values of 5 to 40 cm. The same obstacle profile was used for all runs so that any change in energy was due only to DX variation. The lower curve in figure 3-1 shows the rate of decrease of E with DX . As would be expected for such a calculation, the rate of change is small initially but increases at an increasing rate for large values of DX . The top curve is a plot of the same data in terms of percentage error. A DX value of 10 cm was chosen as being a good compromise between accuracy and computation time.

The parameter, S , can be considered as a measure of repeatability. If an obstacle profile is defined for a very short distance, the presence of one large obstacle could greatly effect the energy. When a new random obstacle path is defined over the same distance, the one large obstacle might not appear so the energy would be much less than before. Obviously, an infinite path length is required for the true energy requirement. Between these two extremes of path

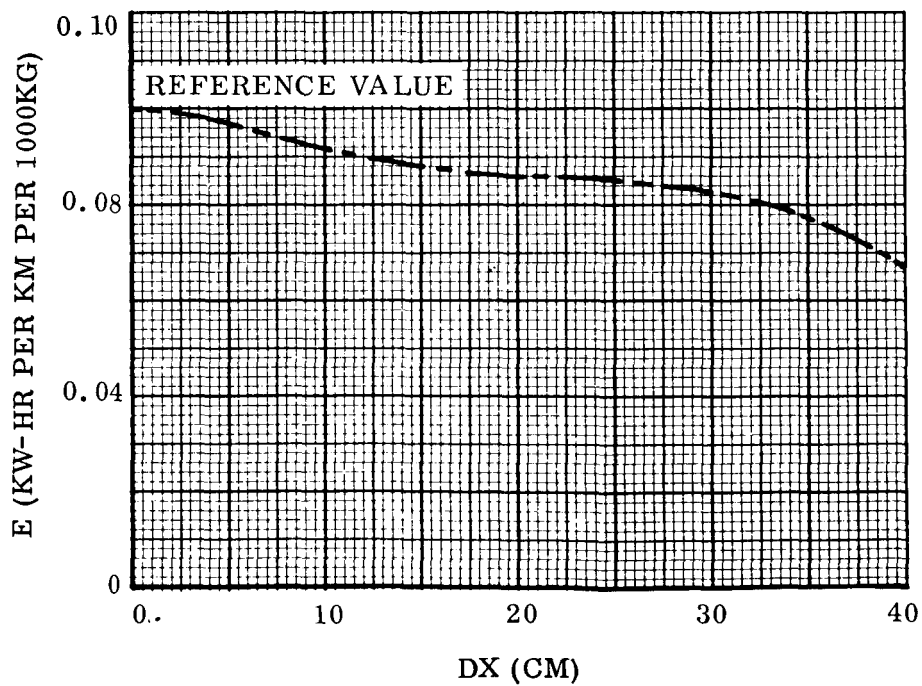
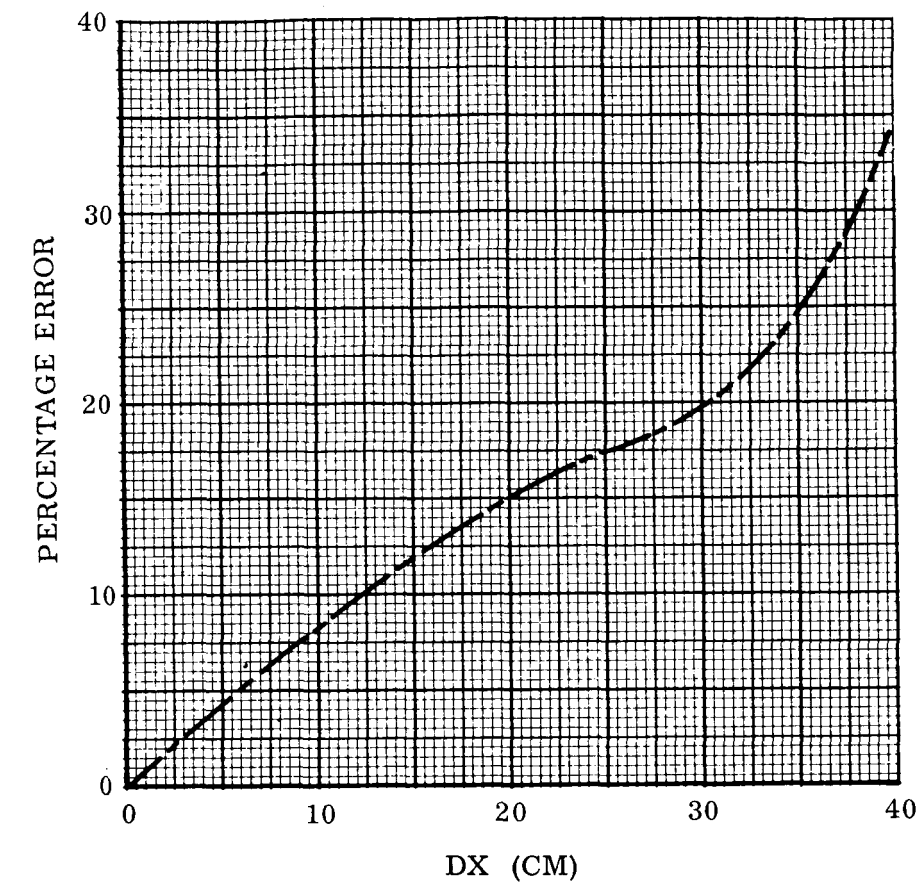


Figure 3-1. Energy Versus Energy Summing Interval

length there can be found some value which gives a reasonable compromise between accuracy and computation time. Figure 3-2 shows the information used in making qualitative choice of an S value. The solid line in figure 3-2 represents E versus C for an infinite path length. A large number of runs were made for path lengths of 1/4, 1/2 and 1.0 km and a 2σ statistical variation computed for each. These 2σ variation boundaries are plotted to show the area in which 95 percent of all points will fall if the energy is calculated repeatedly over different random obstacle profiles for a given S. An S value of 1.0 km was chosen because it presented a good compromise between data scatter and computation time.

Thus, for the parametric data that follows, DX equals 10 cm and S equals 1.0 km. This gives an n value of:

$$n = \frac{100,000}{10} = 10,000$$

This large value of n indicates the reason for preoccupation with computation time.

C. PARAMETRIC DATA

Reviewing Equations (1) and (12) will show what parameters were considered parametrically.

$$Y = Y_{\max} (RN)^C \quad (1)$$

and

$$E = \sum_{n=0}^n \left[\sum_{j=1}^{NW} (H_{j,n+1} m_j) - \sum_{j=1}^{NW} (H_{j,n} m_j) \right] \quad (12)$$

The value of n has been fixed; WB has negligible effect; and m is constant at 1000kg per wheel. This leaves DI, C, Y_{\max} , NW, and D to be treated parametrically.

(1) E variation with C. The primary form of data presentation in this report is a plot of E versus C for various values of D. Figure 3-3 shows such a plot with a D variation from 100 to 250 cm. This plot is for a two-axle vehicle with a DI of 20 cm and a Y_{\max} of 100 cm. Figure 3-4 is a similar plot for three axles and shows a small decrease in energy.

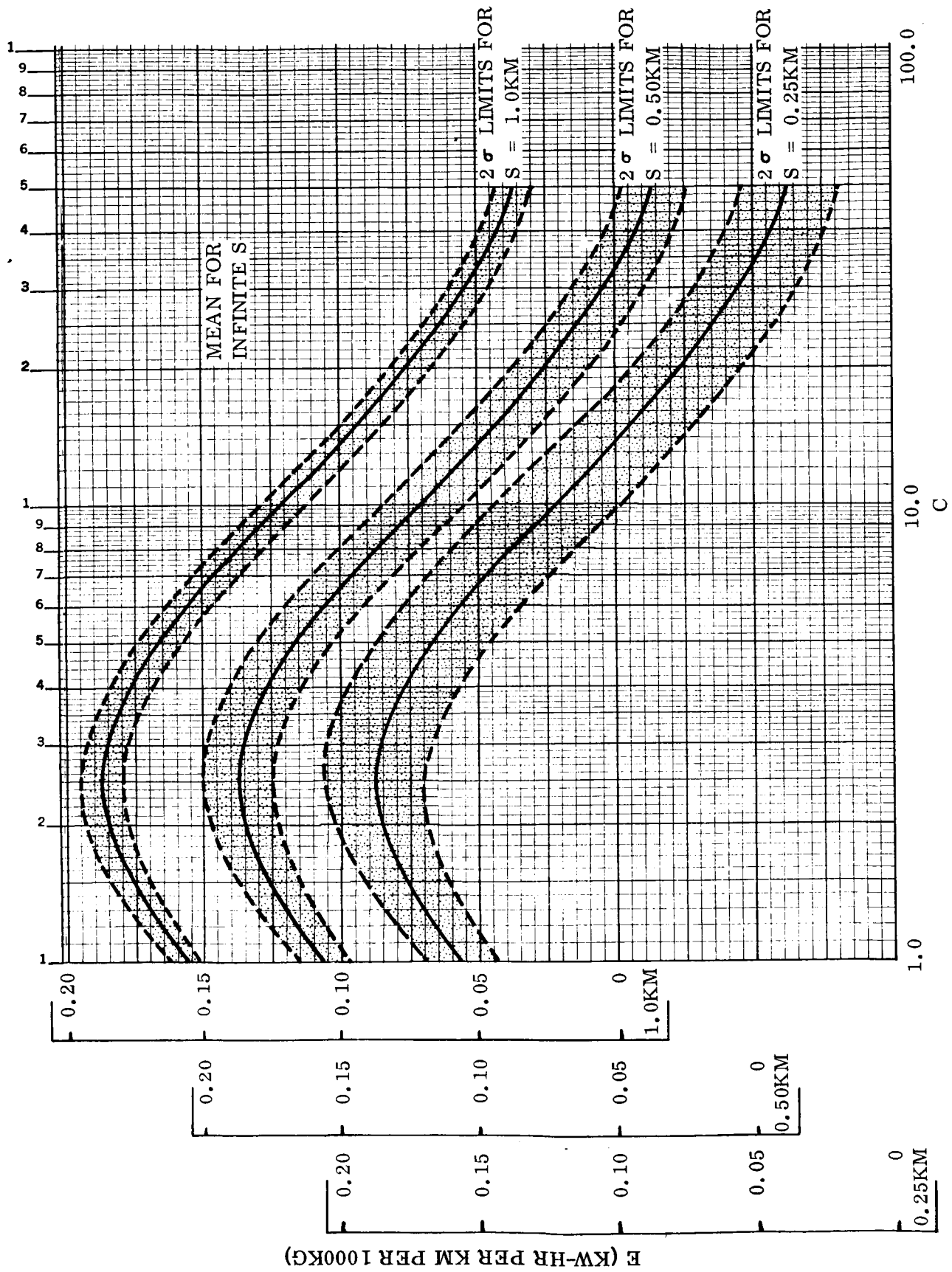


Figure 3-2. 2 σ Variation for Various Distances Traveled

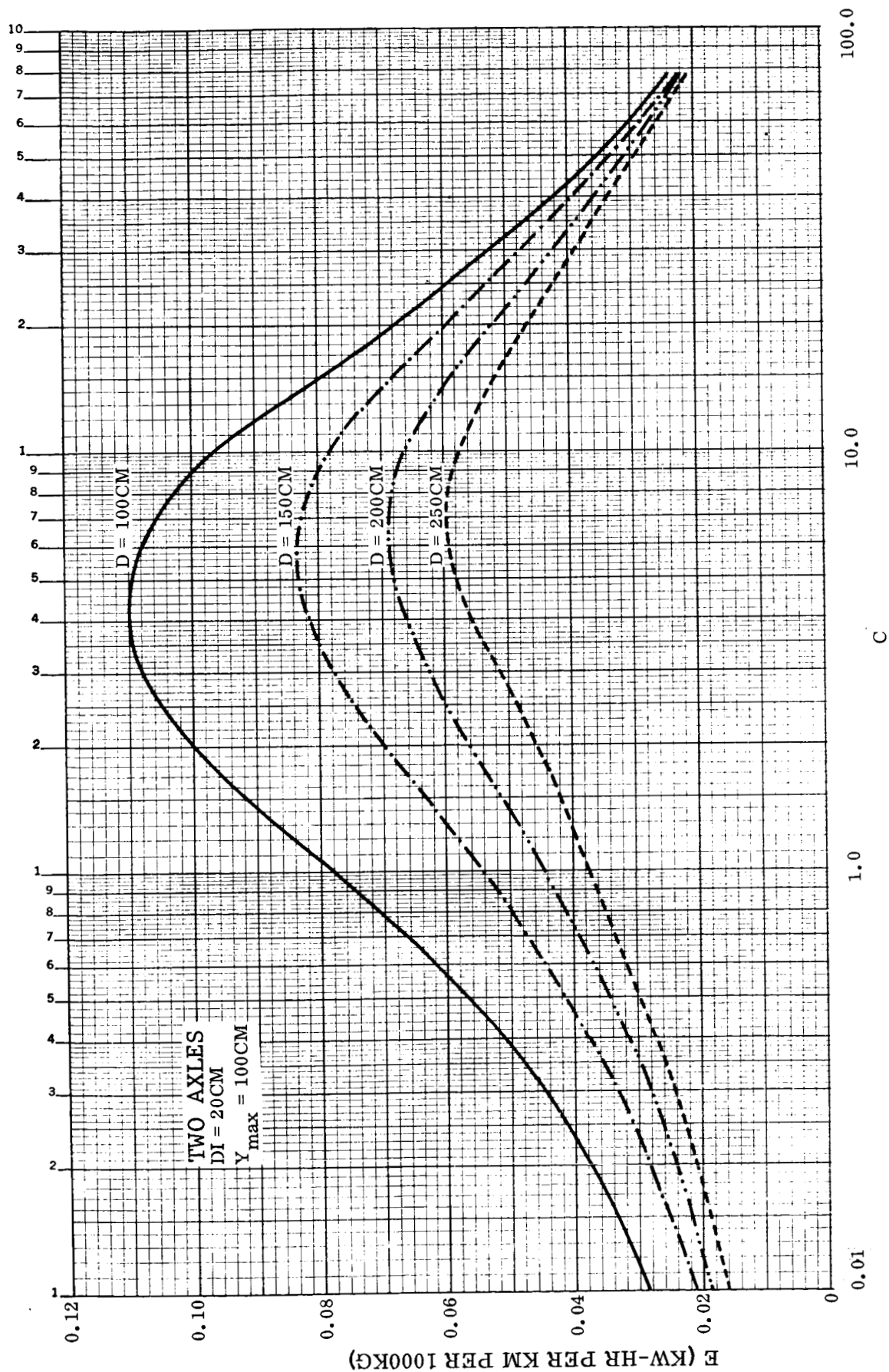


Figure 3-3. Energy Versus C for Various Wheel Diameters

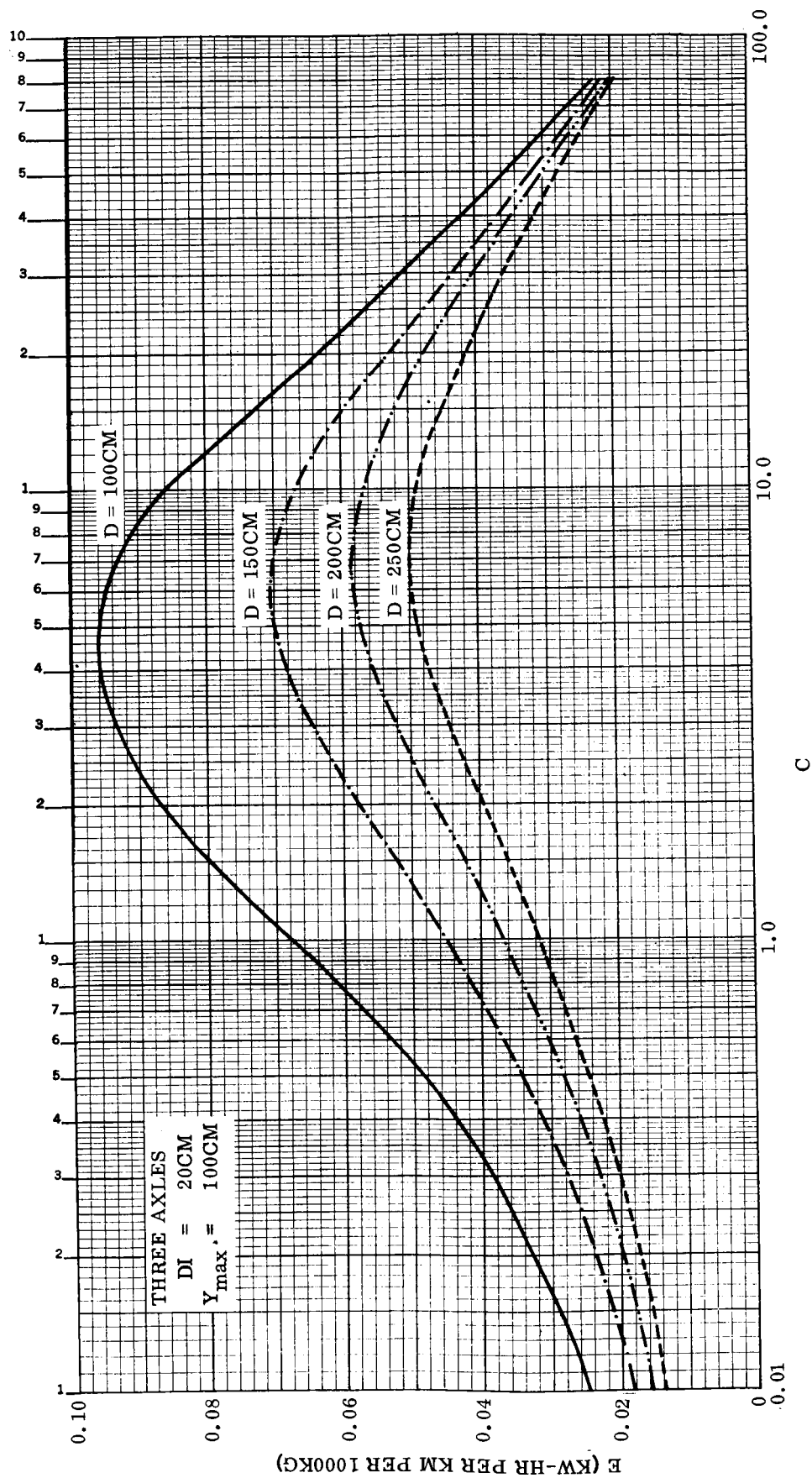


Figure 3-4. Energy Versus C for Various Wheel Diameters (Three Axles)

These figures are typical of the data generated. The appendix includes additional data for DI values of 5, 10, 20, 40 cm and Y_{\max} values of 25, 100, 175 and 250 cm. Some scatter was present in the plotted data; however, enough points were run to make possible a good average fairing. One caution should be taken when using the data. Since the maximum obstacle height that a vehicle can negotiate is dependent upon the vehicle layout and Lunar surface characteristics, some combinations of D and Y_{\max} used in this report might be unrealistic. When determining energy requirements from this data, a realistic combination of D and Y_{\max} should be established rather than using the worst case.

(2) E Variation with DI. Figure 3-5 illustrates how the point of maximum energy shifts with a change in DI. Note that there is no change in the magnitude of maximum energy. But, for a given C , E decreases rapidly with increasing DI. This is due to the fact that fewer obstacles are defined over one km for larger DI values.

(3) E Variation with Y_{\max} . Intuitively, it seems that energy should be directly proportional to Y_{\max} . Figure 3-6 shows this to be true. Also shown is the decrease in rate of change with an increase in D . Two points can be made concerning this plot. First, the data is for a C of 8. Referring to figure 3-5 shows that for a DI of 20 cm peak energy is near a C of 8. This means that an energy value from figure 3-6 will allow a vehicle to negotiate profiles for all C values.

The second point is that energy requirements become very large for some conditions. If the rule-of-thumb is used which says that a two-axle vehicle can negotiate obstacles up to $1/3 D$, the highest value of E possible is .05, a low value. The range of values used is not meant to indicate upper limits but to cover all possible combinations.

(4) E Variation with D . Figure 3-7 gives the same data discussed above replotted to show the E versus D variation. For very small Y_{\max} values, the energy is insensitive to D , but, as Y_{\max} increases, D has more effect. From the obstacle negotiation standpoint, use the largest possible D .

(5) E Variation with NW. Figure 3-8 shows in bar chart form the E for from one to eight axles. The data shows a 50-percent reduction in energy requirement going from one to eight axles. In actual practice, this reduction would be tempered by an increasing drive train energy loss for such a large number of axles.

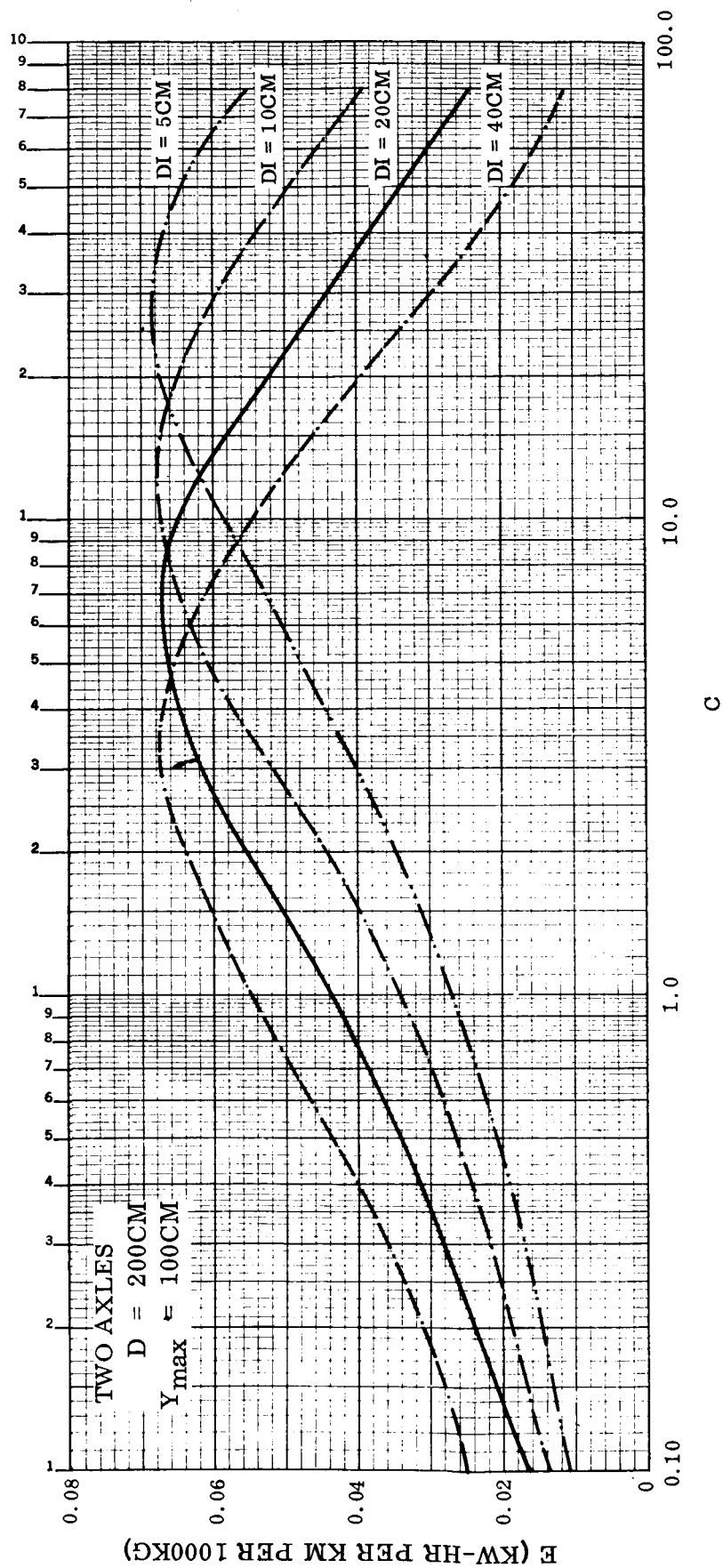


Figure 3-5. E Versus C for Various Values of DI

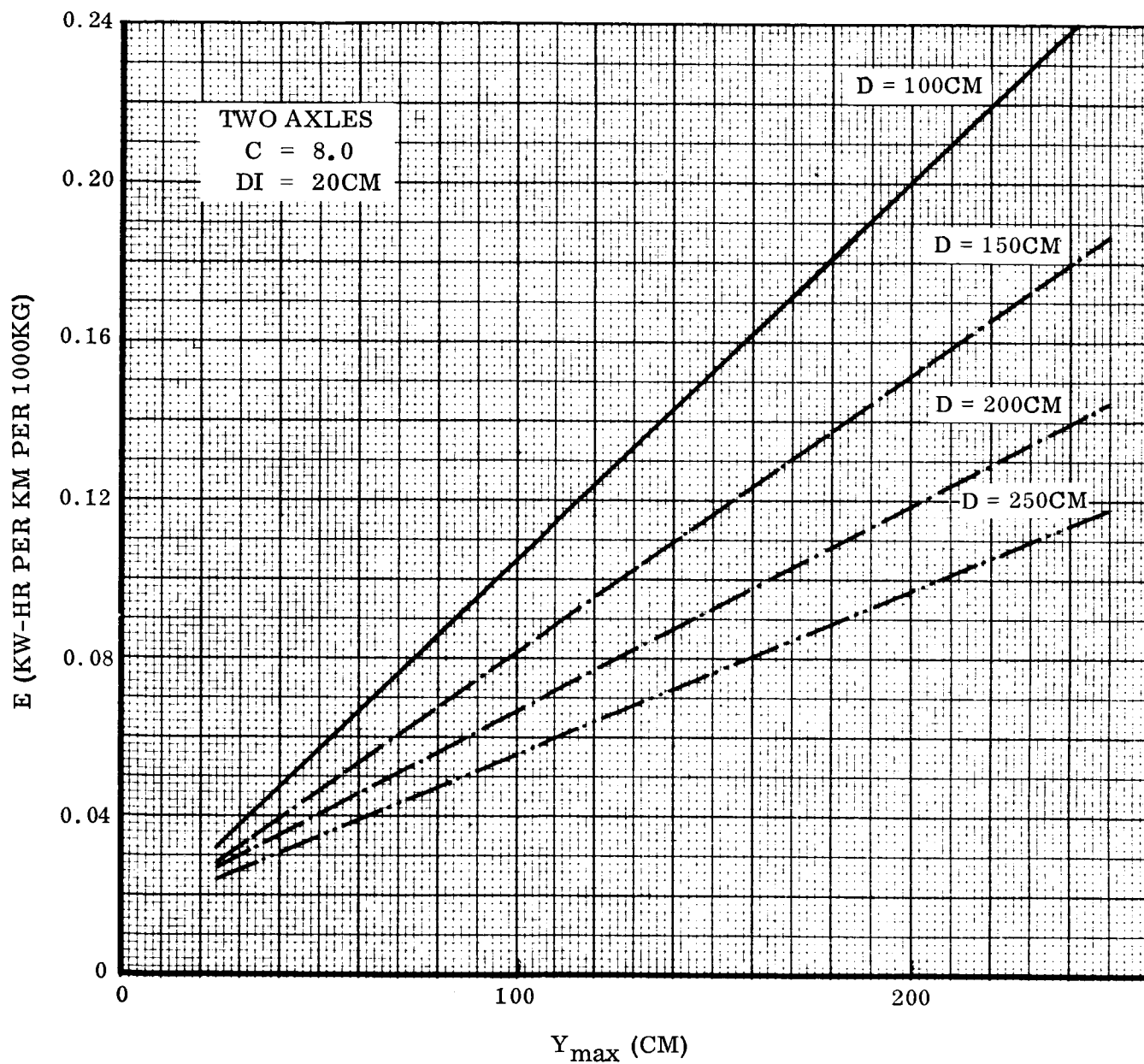


Figure 3-6. E Versus Y_{max} for Various Values of D

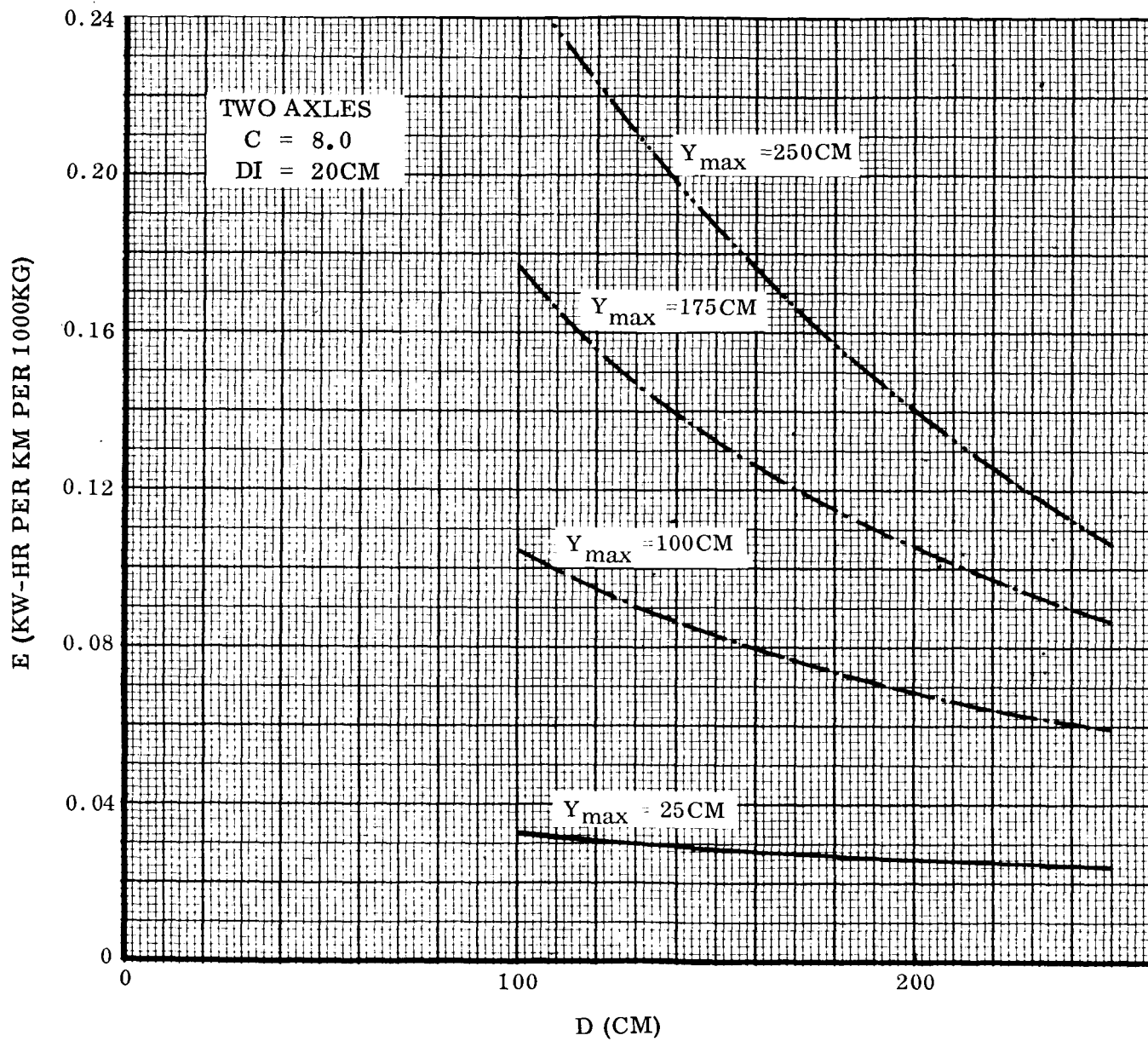


Figure 3-7. E Versus D for Various Values of Y_{\max}

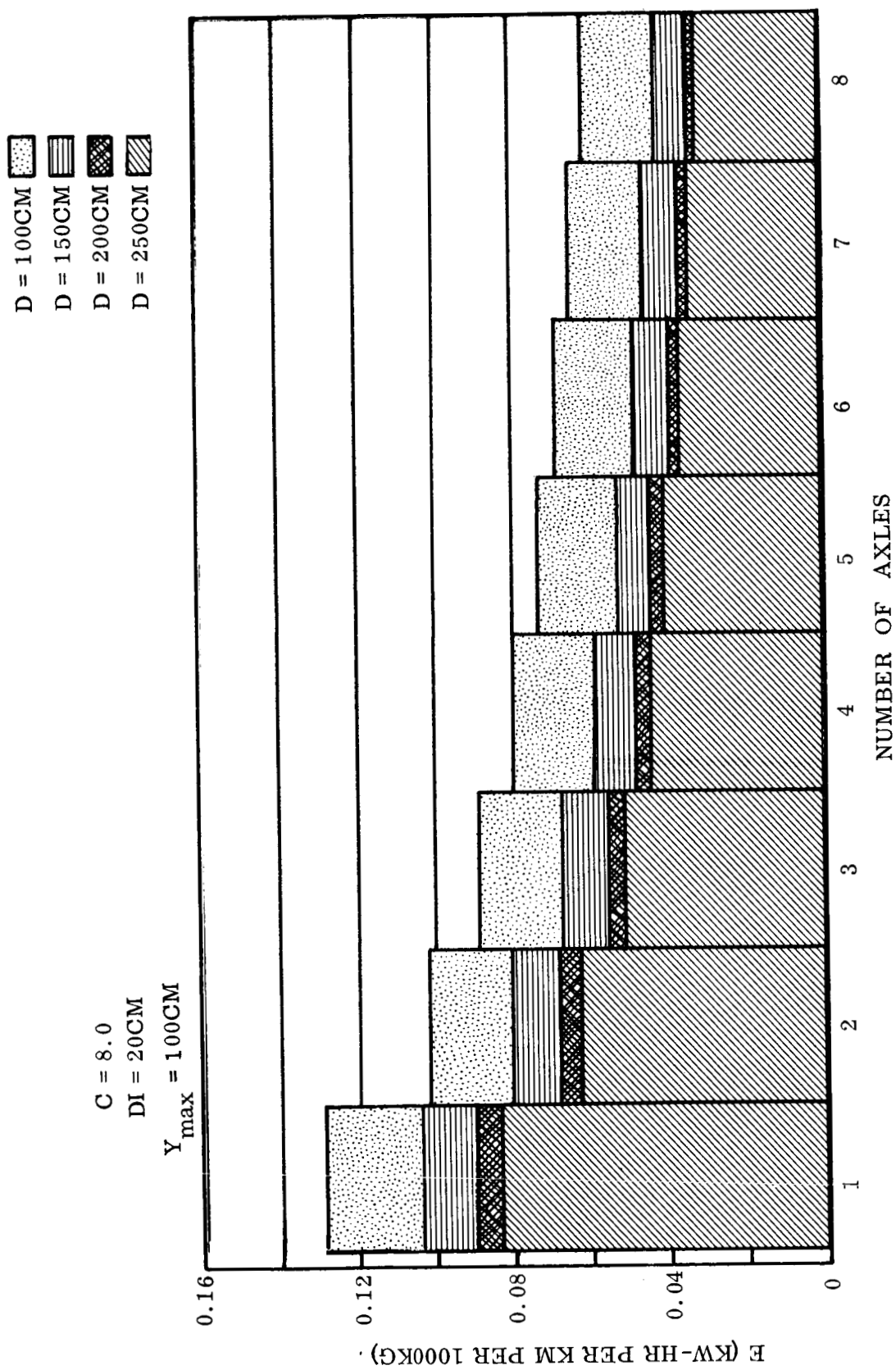


Figure 3-8. E Versus Number of Axles for Various Values of D

(6) E Variations with Mass Distributions. All energy calculations were based on the assumption that an equal mass acted through the center of each wheel. Figure 3-9 depicts the effect of altering the mass distribution for two and three axles with an assumed total vehicle mass of 2700 kg. The plot is E versus the percentage of total vehicle mass acting on the first axles. Curves are shown for various distributions between the remaining two axles. The R_2 equals 100 percent curve is a two-axle vehicle, since the mass on the third axle is zero.

For two axles the minimum energy is obtained with 50-percent mass on each axle. For three axles, the minimum energy occurs at 35-percent mass on the first axle and even distribution of the remaining mass between axle two and three. Since the data presented in this report is for even distribution, it would give a value of E as marked X, showing that even distribution is very nearly minimum.

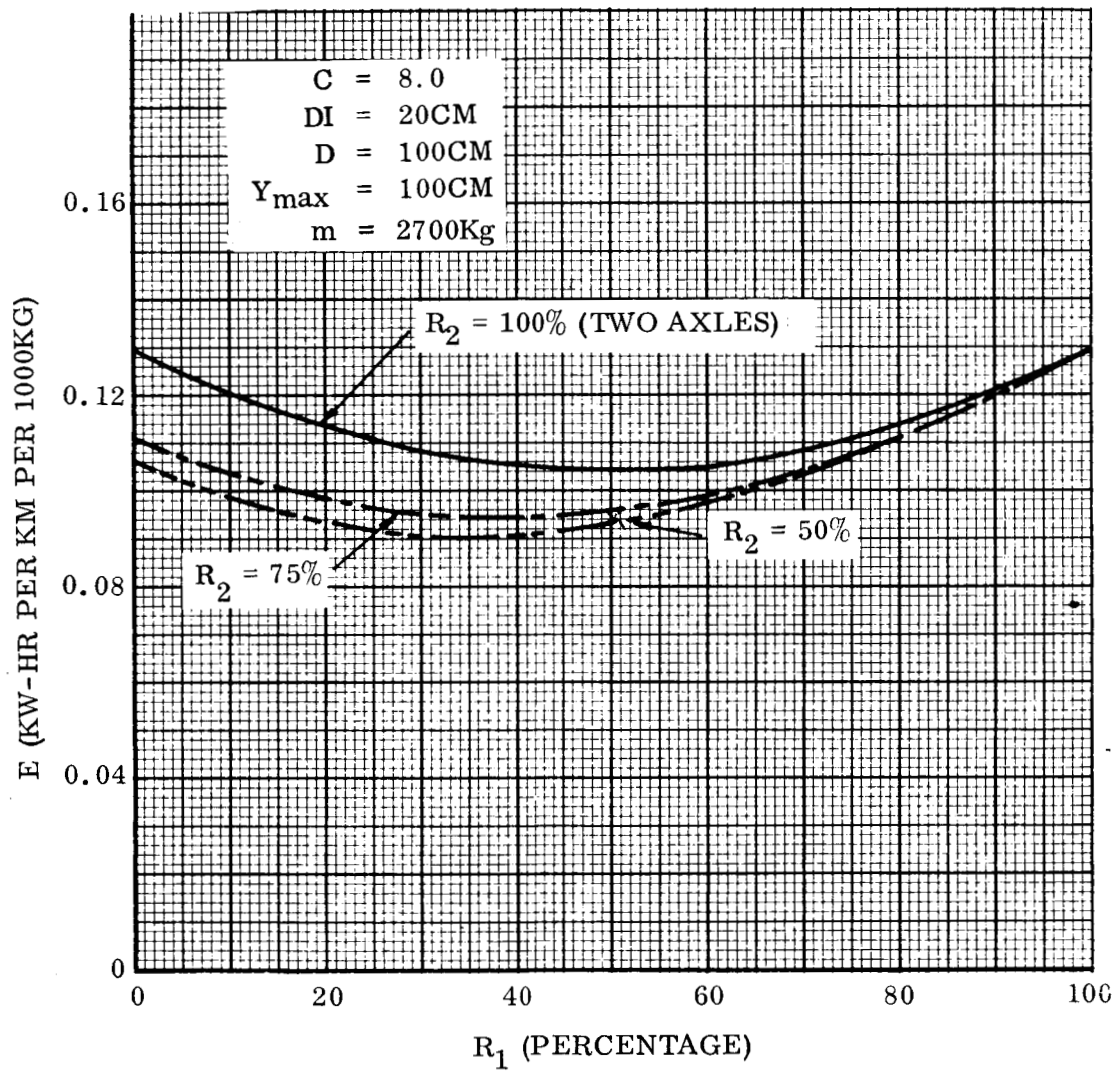


Figure 3-9. Energy Variation with Weight Distribution for Two and Three Axles

SECTION IV ANALYSIS OF DATA

A. GENERAL

At this point, the major question; "What is the energy requirement for negotiating obstacles?", is still not answered. The parametric data has shown that the variation of energy with the parameters considered is so complex that it is impossible to choose one all-encompassing value. In the following discussion, a typical vehicle will be evaluated by using the parametric data presented.

Following is a list of the assumed vehicle characteristics:

Vehicle Mass	3000 kg (~ 6500 lb)
No. of Axles	2
Wheel Diameter	200 cm (~80 in)
Drive Train Efficiency	.6
Energy Required for Mobility (ELMS)	.30 $\frac{\text{kw-hr}}{\text{Km}}$

Equal Mass Distribution

B. DETERMINATION OF ENERGY FOR OBSTACLES

It is necessary to choose values for three parameters that define an obstacle profile. Obstacle spacing will be arbitrarily chosen as 20 cm. Maximum obstacle height will be 50 cm. This is probably the highest obstacle that the vehicle would attempt to go over. The final value, distribution exponent, C, is more difficult to determine. Since this is such an important parameter, energy required for obstacles was determined for a wide range of C values. This data is plotted in figure 4-1 as a percentage of energy for mobility versus C. For this assumed case, the 20 percent recommended by TR-83-D is sufficient for only a C of 80. Referring back to the obstacle frequency numbers of figure 1 shows that a profile with C of 80 will probably be rough enough. But, due to the lack of experience in the use of C, the value chosen should be conservative. If C is reduced to 40, which gives a much rougher surface, energy for obstacles increases to 35 percent. This value could be used rather than the recommended 20 percent to allow for some built-in conservatism.

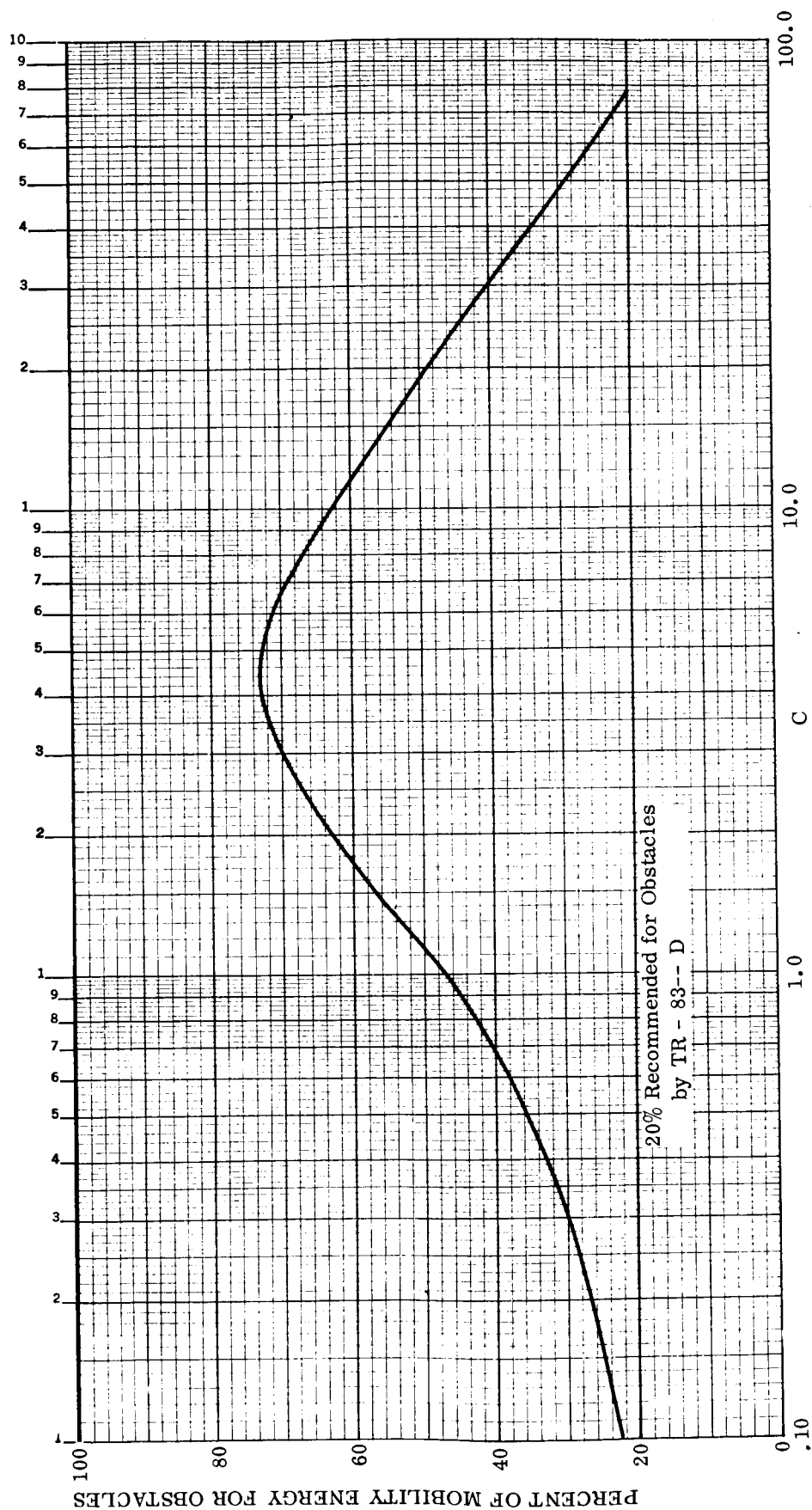


Figure 4-1. Percent of Mobility Energy for Obstacle Negotiation Versus C From Sample Problem

SECTION V

CONCLUSIONS AND RECOMMENDATIONS

A. GENERAL

This completes the presentation of an analytical method for determining energy required for obstacle negotiation. It has been obvious in certain areas that alternative methods could have been used. The direction taken was the best possible with present knowledge but new directions might be dictated by future developments. The basic philosophy behind the method is sound and can be used in future mobility analyses.

B. CONCLUSIONS

The primary conclusion to be drawn from the parametric data is that the value of energy for obstacle negotiation is of such a magnitude as to require its inclusion as an integral part of the mobility analysis and not treat it as a reserve. This can be done by superimposing an obstacle profile on top of a macro-profile such as defined in TR-83-D. If a reserve is to be used, the 35-percent value is probably better than 20 percent. When a three-dimensional analysis is required, two obstacle profiles can be defined simultaneously.

C. RECOMMENDATIONS

The area that obviously requires additional effort is the correlation of the distribution exponent, C , to some real obstacle distributions. This is possible by using terrestrial topographical charts of areas similar to areas of interest on the Lunar surface. Distributions of obstacle heights can be determined and compared to distributions for various C values. As Lunar surface profile data becomes available, even more accurate C values can be determined.

APPENDIX

The appendix presents the results of the parametric analysis in the form of energy versus C plots. Figures A-1 through A-13 give data for wheel diameters of 100, 150, 200, and 250 cm; maximum obstacle heights of 25, 50, 75, and 150 cm, obstacle spacing of 5, 10, 20 and 40 cm; and for two- and three-axle vehicles. The same line coding for wheel diameter is used throughout. Note that the energy scale changes. This was necessary to give sufficient accuracy.

The following legend is applicable to all figures of this appendix:

D	-	CM
100	—	
150	— · —	
200	— · · —	
250	— — —	

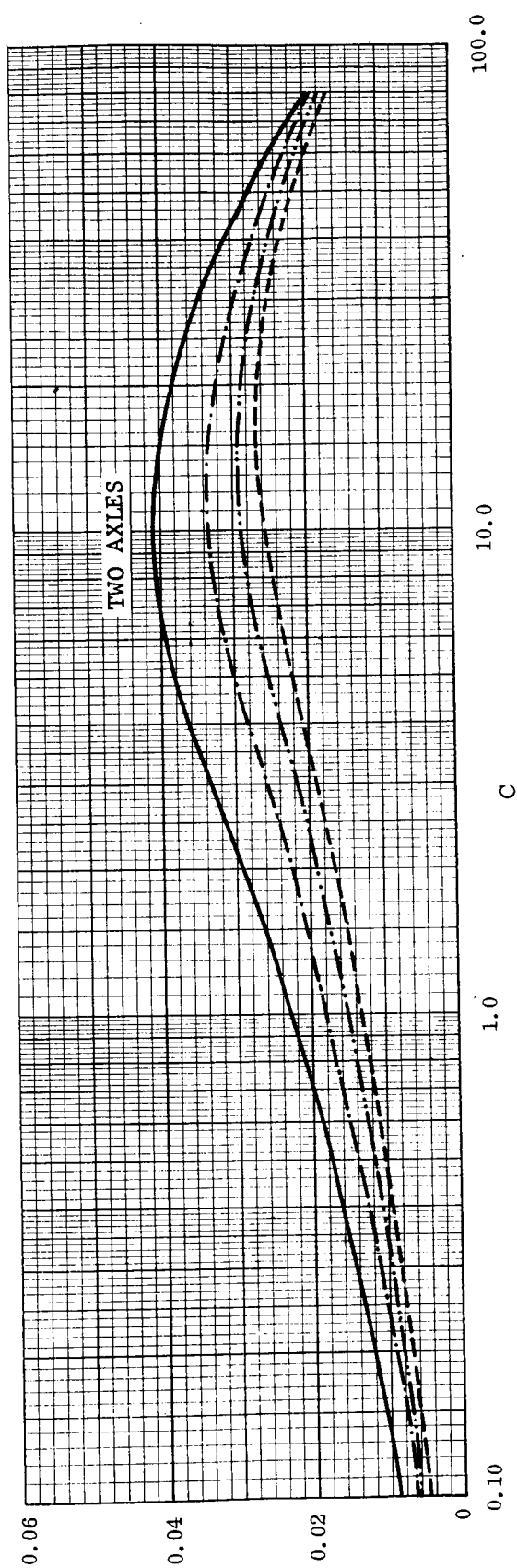
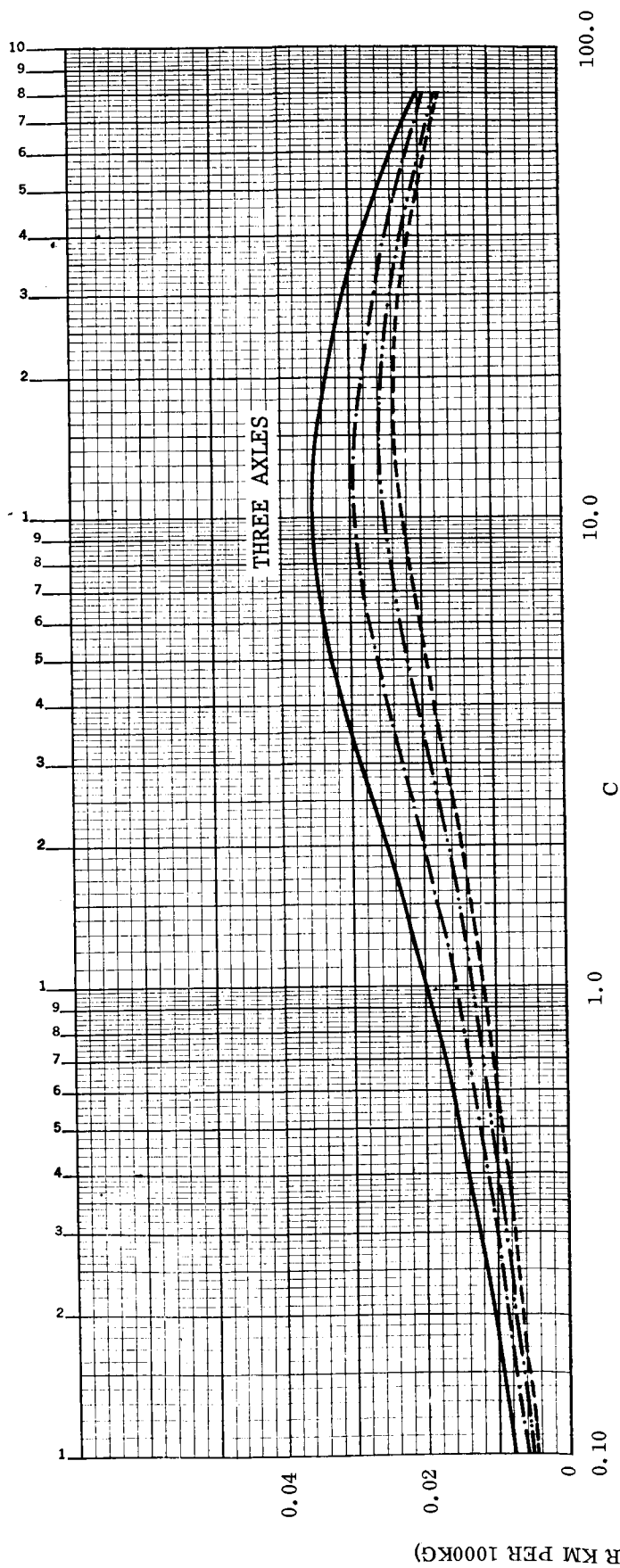


Figure A-1. $DI = 5\text{cm}$, $Y_{\text{max}} = 25\text{cm}$

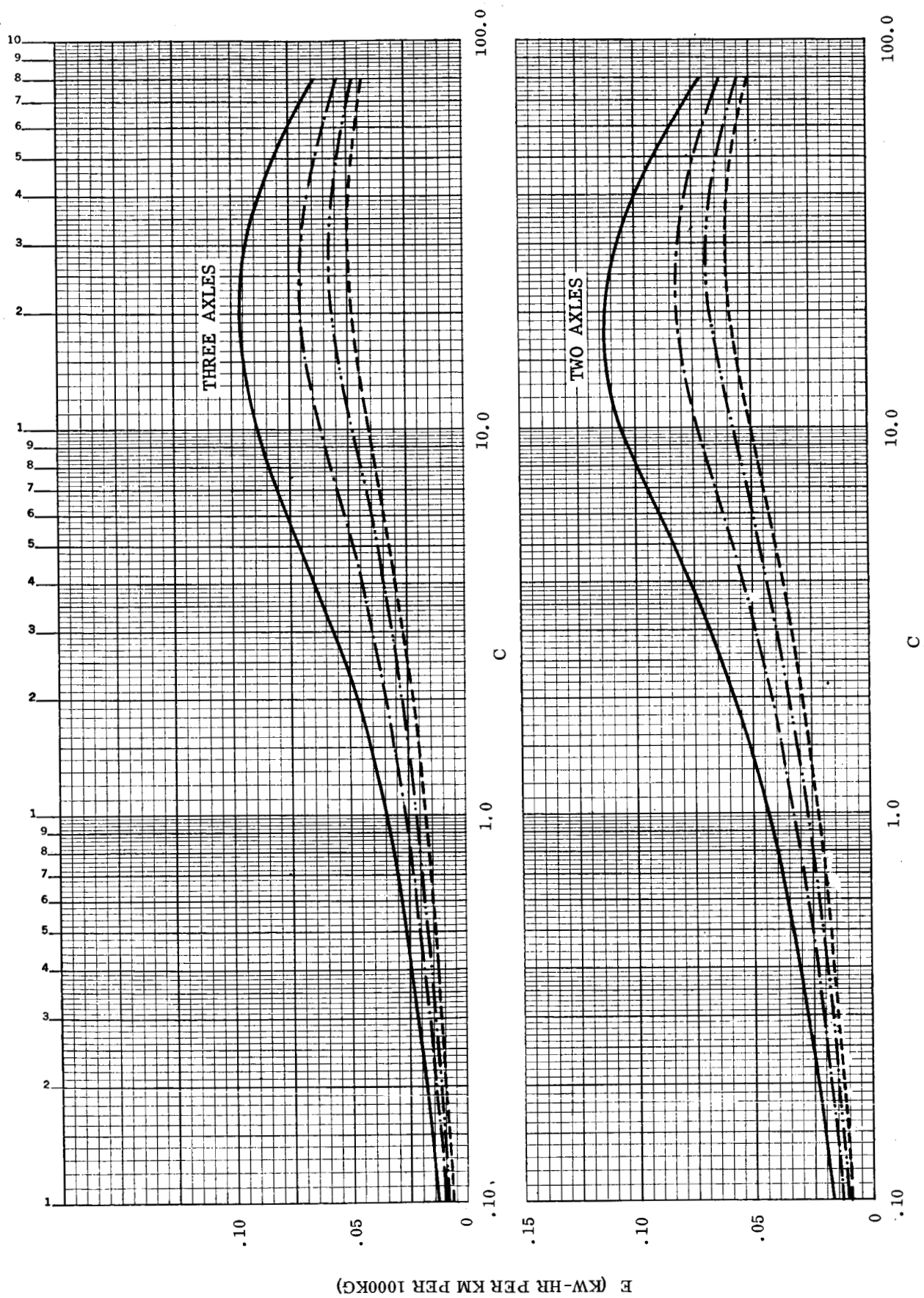


Figure A-2. $DI = 5\text{cm}$, $Y_{max} = 100\text{cm}$

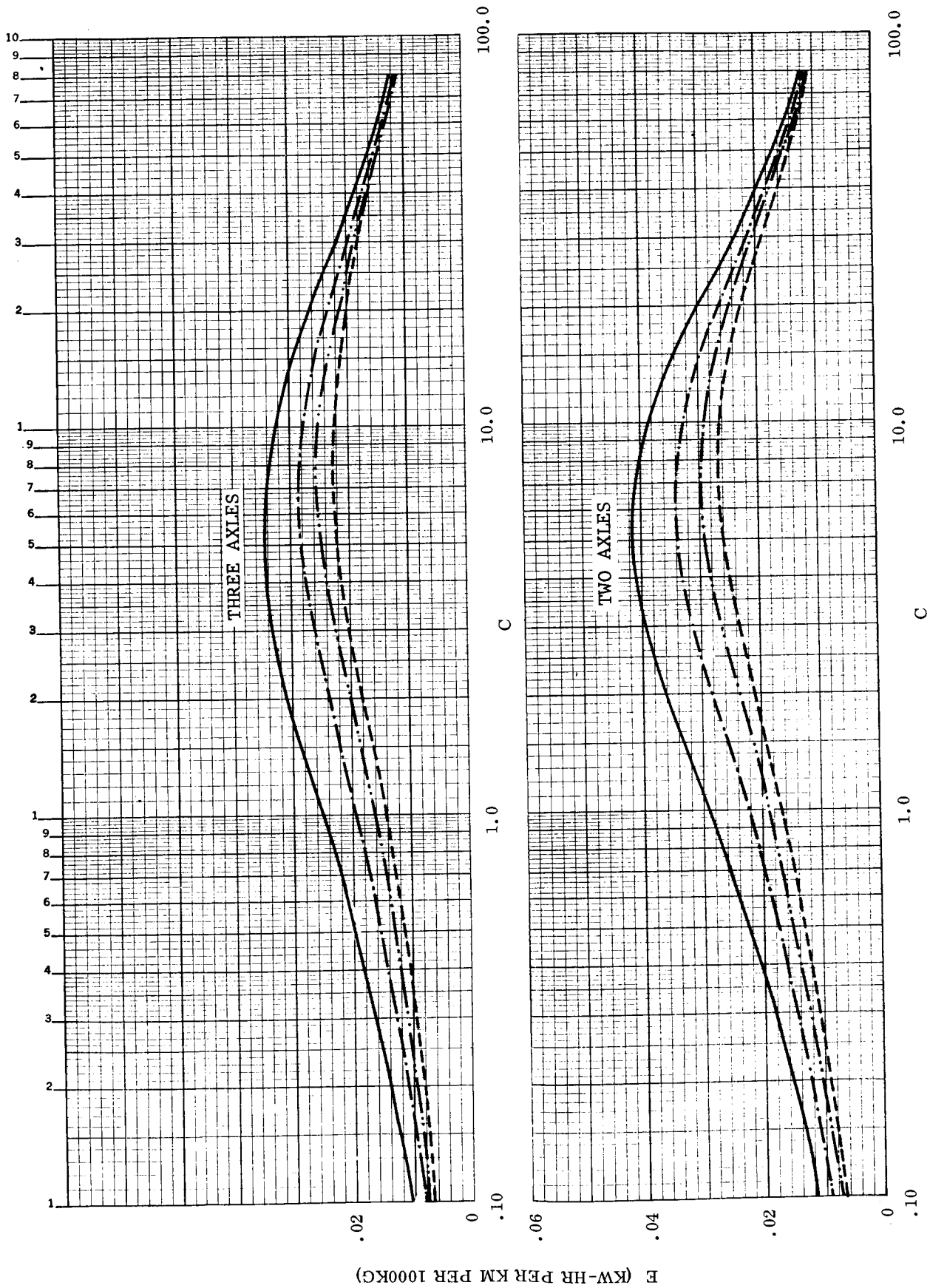


Figure A-3. $DI = 10\text{cm}$, $Y_{max} = 25\text{cm}$

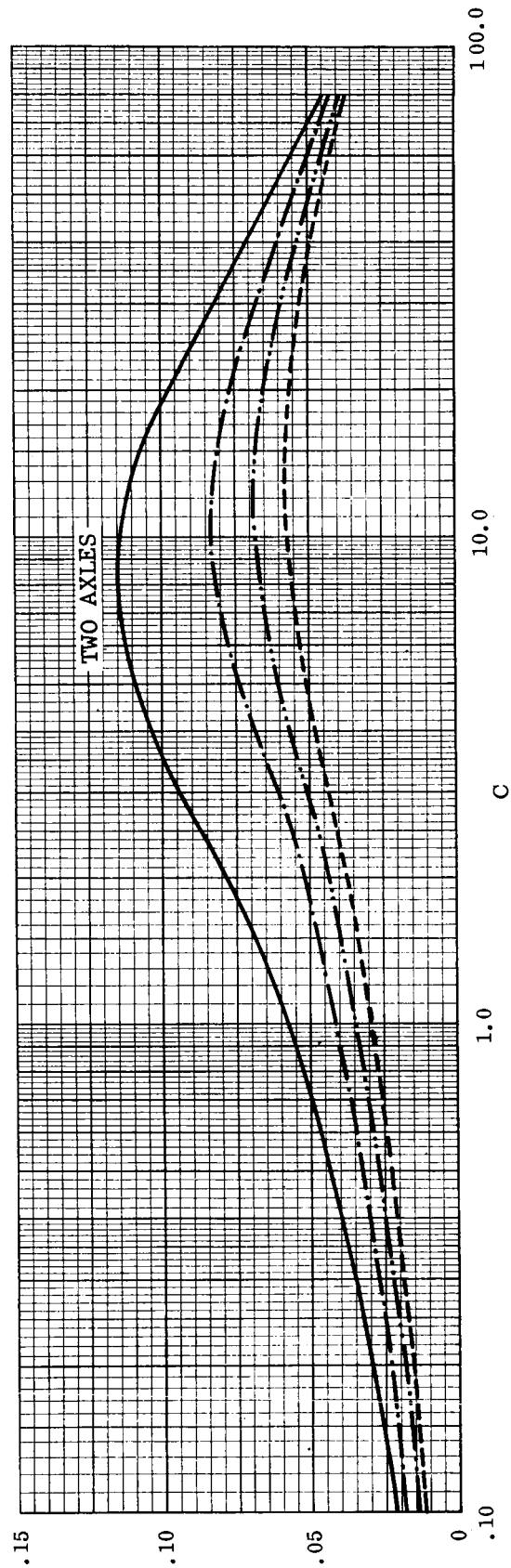
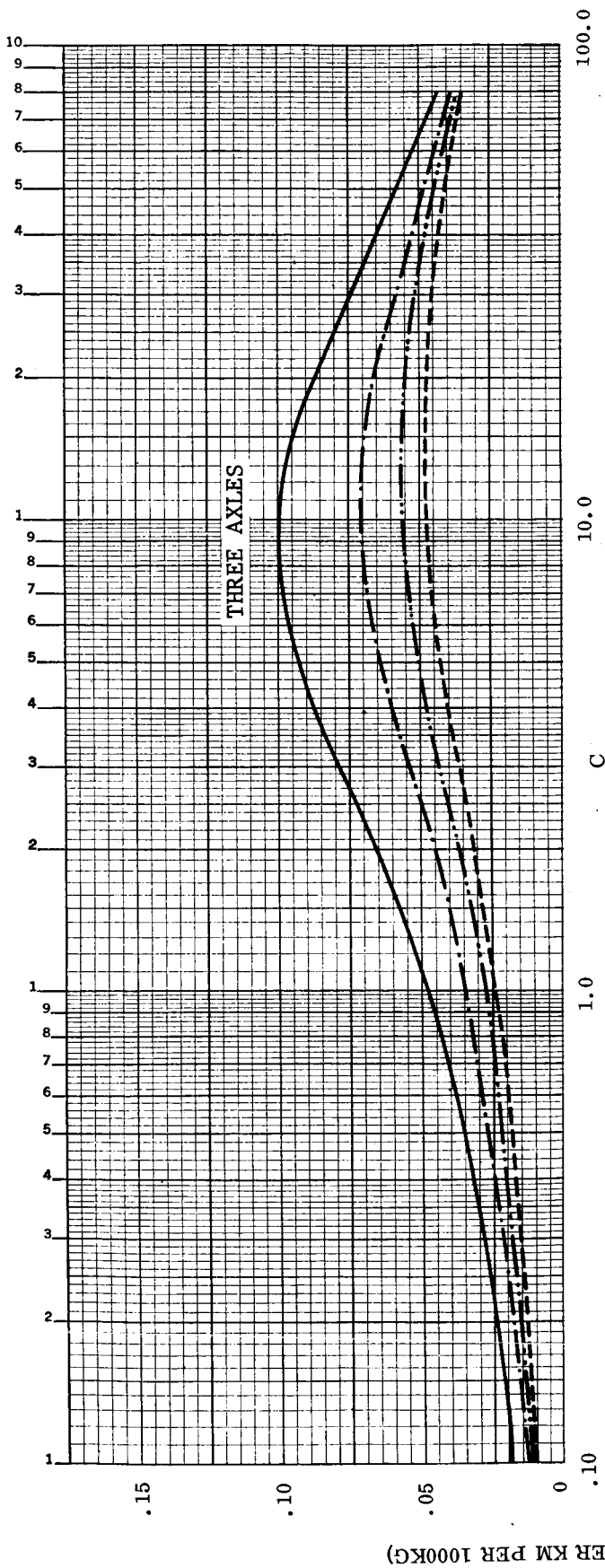


Figure A-4. $DI = 10\text{cm}$, $Y_{\max} = 100\text{cm}$

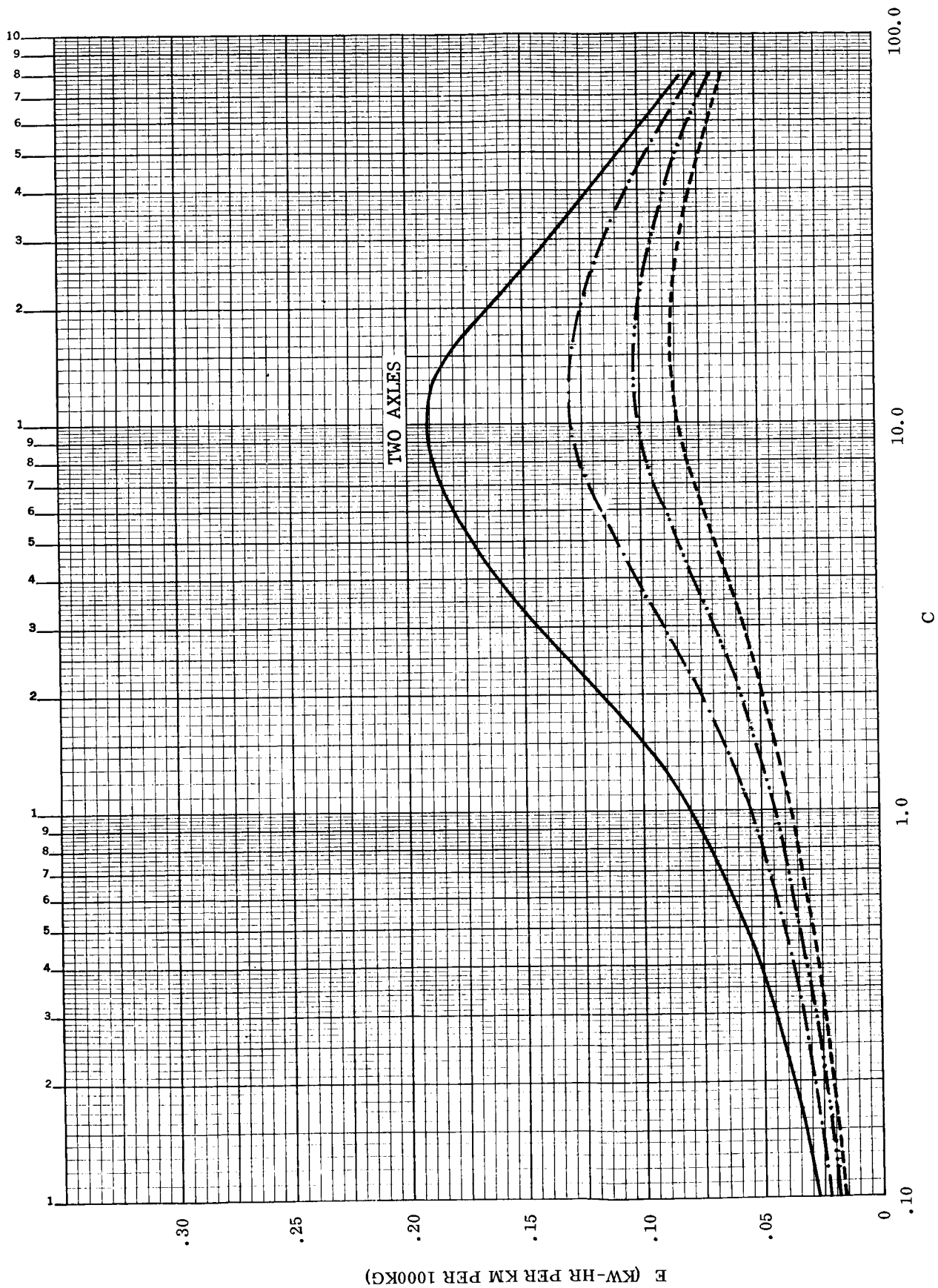


Figure A-5. $DI = 10\text{cm}$, $Y_{\max} = 175\text{cm}$ (Sheet 1 of 2)

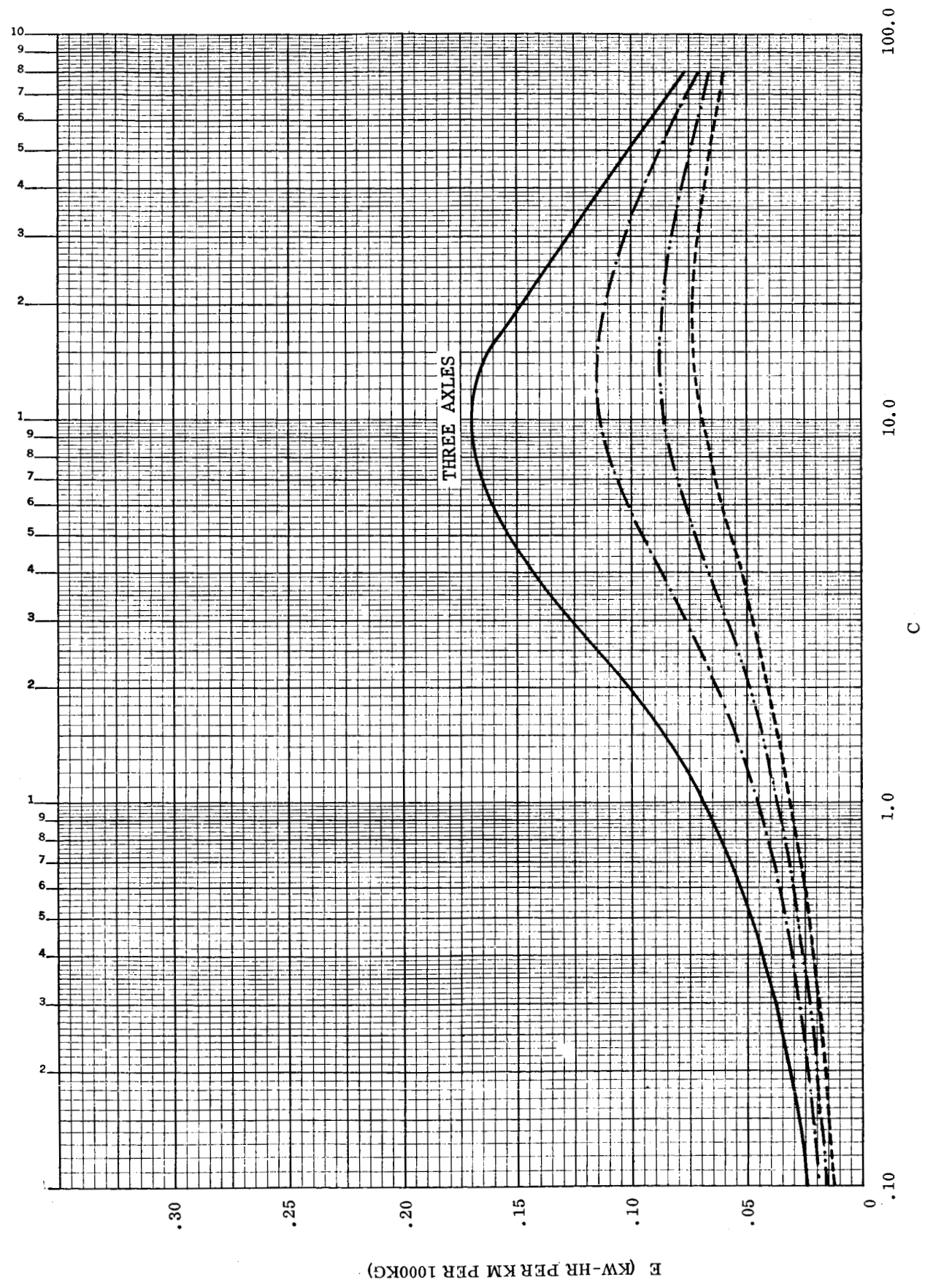


Figure A-5. $DI = 10\text{cm}$, $Y_{\text{max}} = 175\text{cm}$ (Sheet 2 of 2)

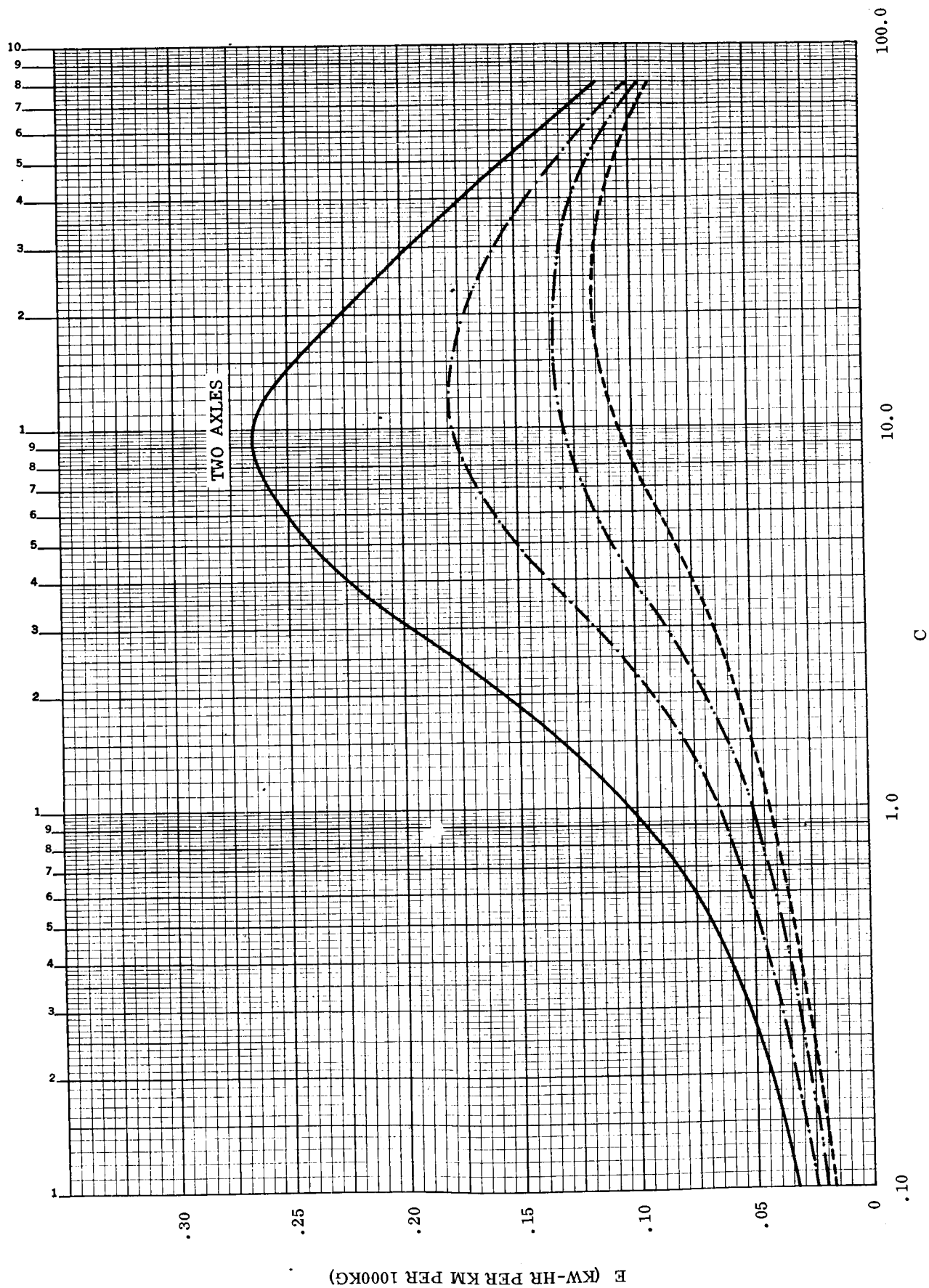


Figure A-6. $DI = 10\text{cm}$, $Y_{\text{max}} = 250\text{cm}$ (Sheet 1 of 2)

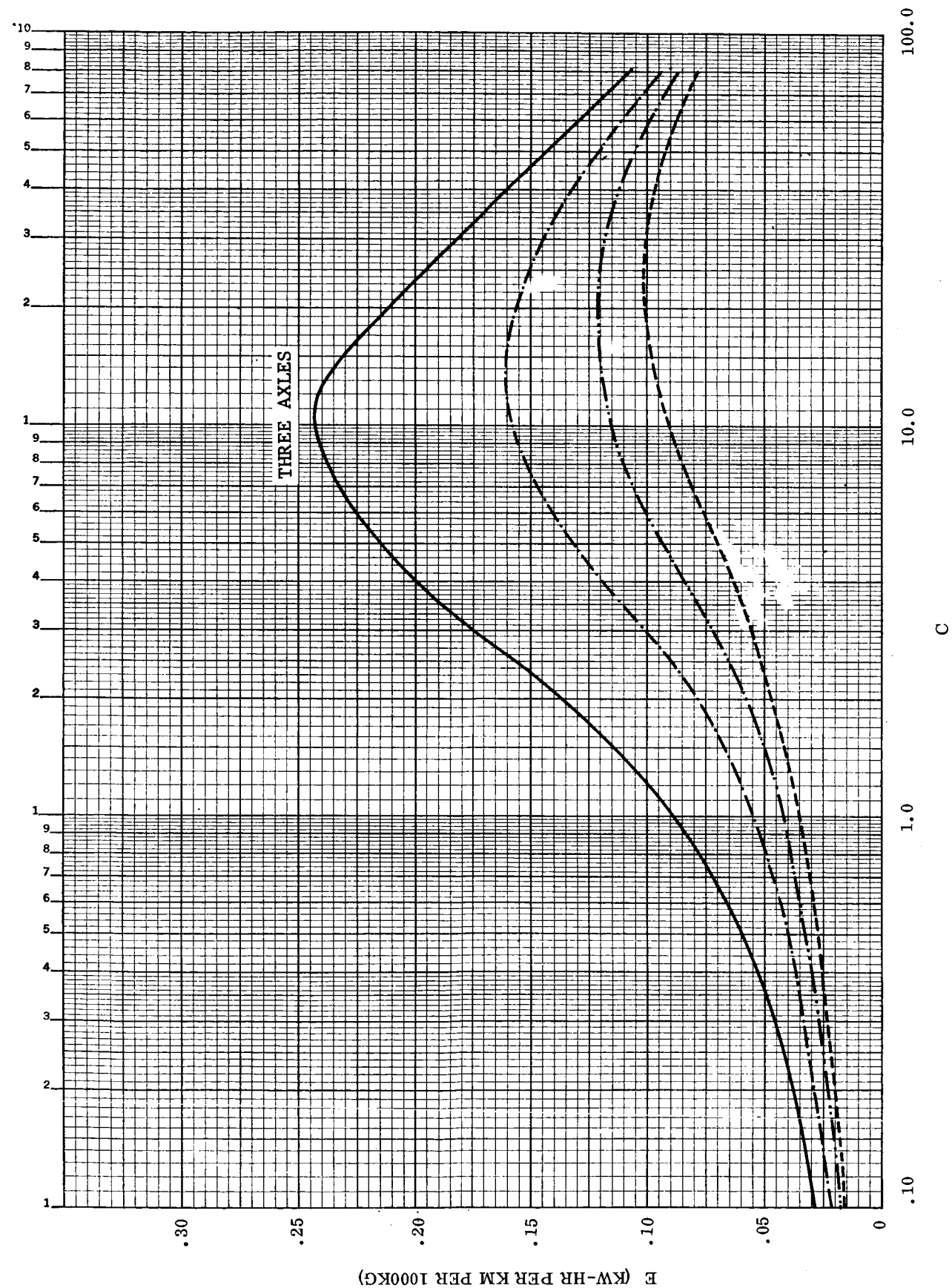


Figure A-6. $DI = 10\text{cm}$, $Y_{\max} = 250\text{cm}$ (Sheet 2 of 2)

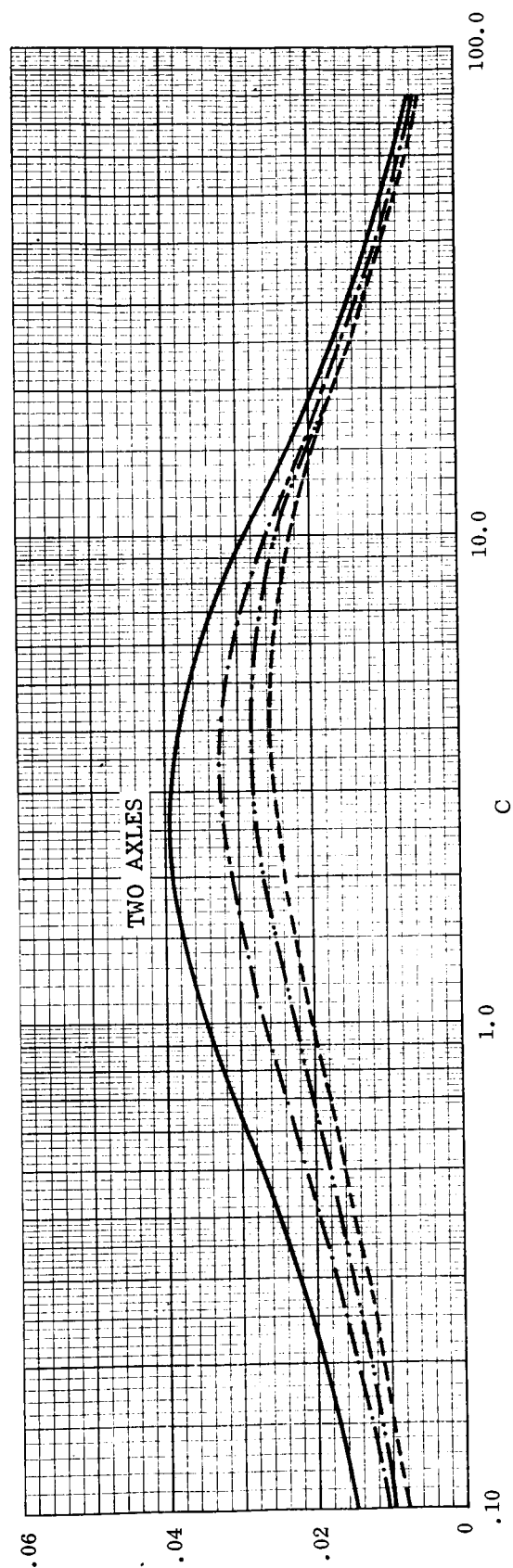
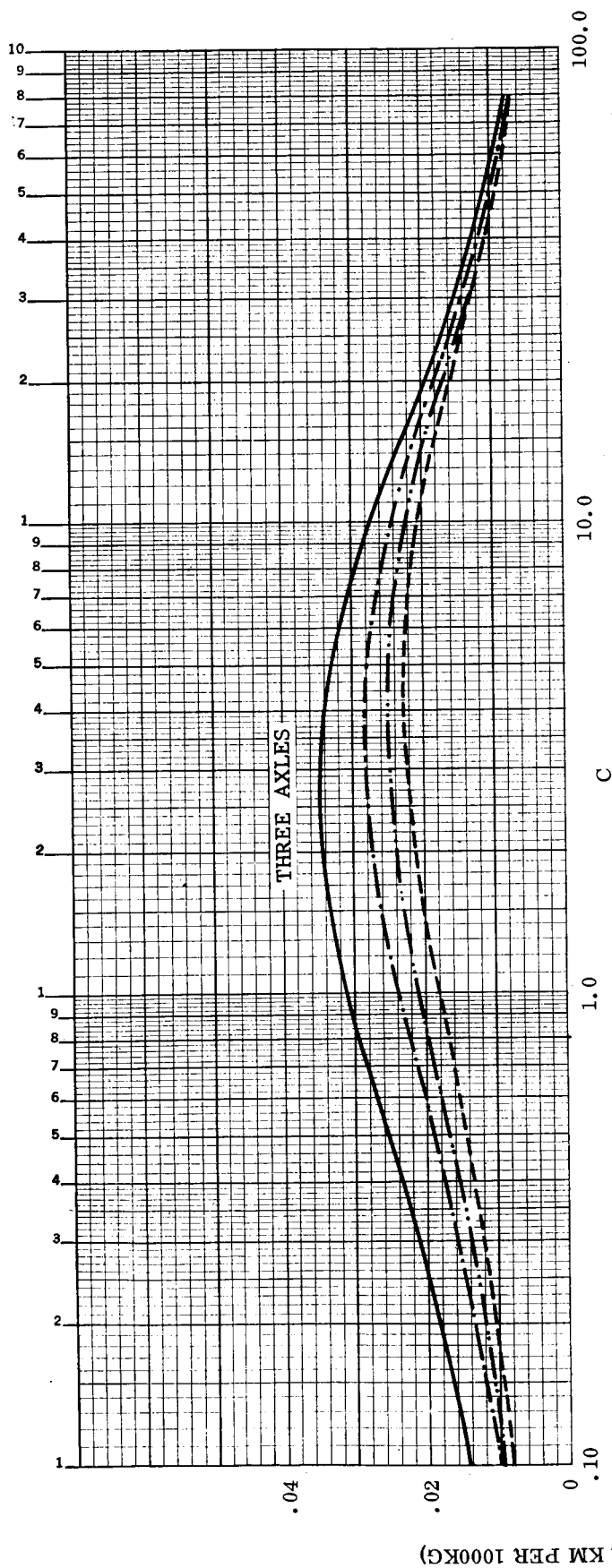


Figure A-7. DI = 20cm, $Y_{max} = 25\text{cm}$

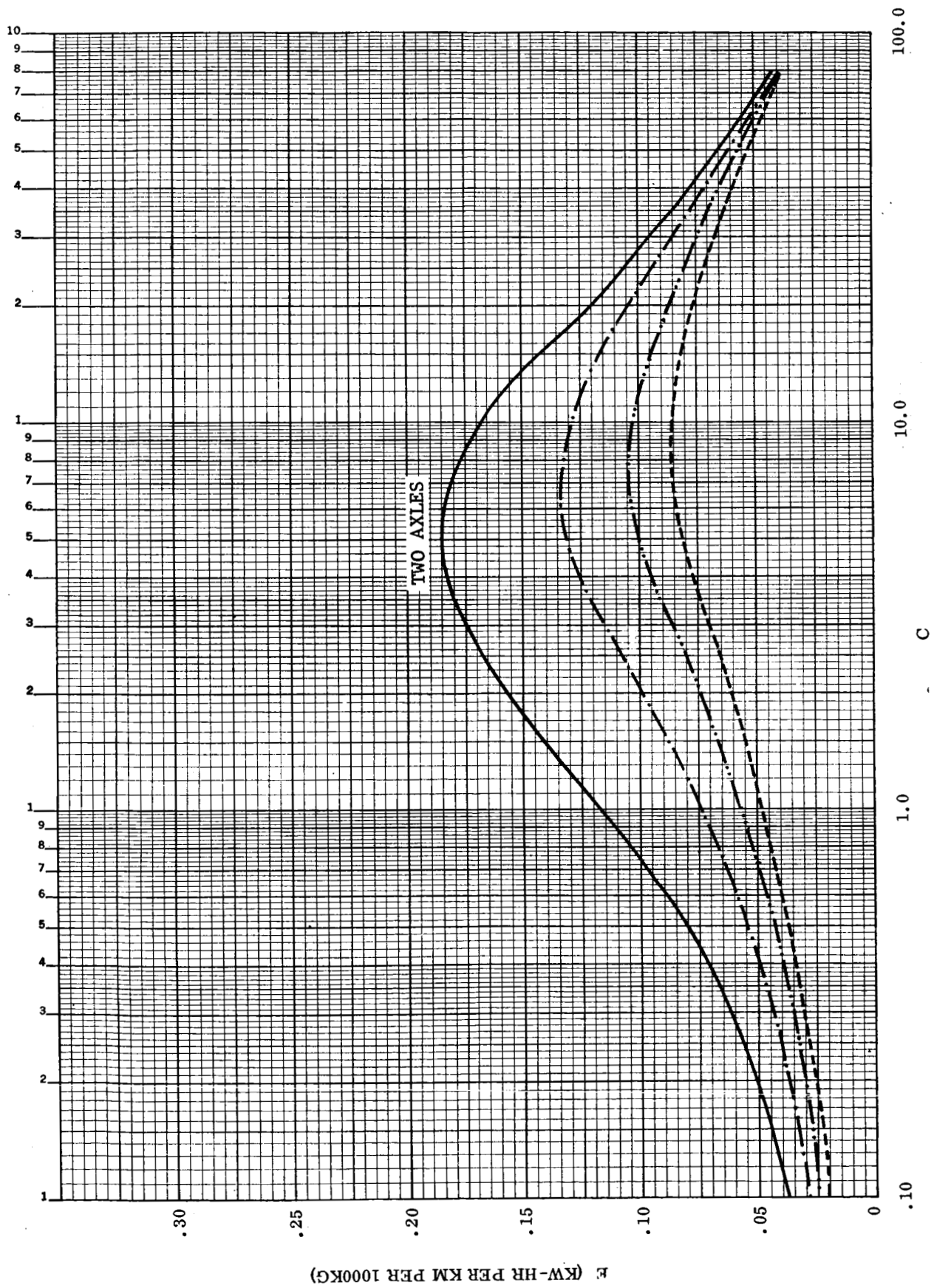


Figure A-8. $DI = 20\text{cm}$, $Y_{\max} = 175\text{cm}$ (Sheet 1 of 2)

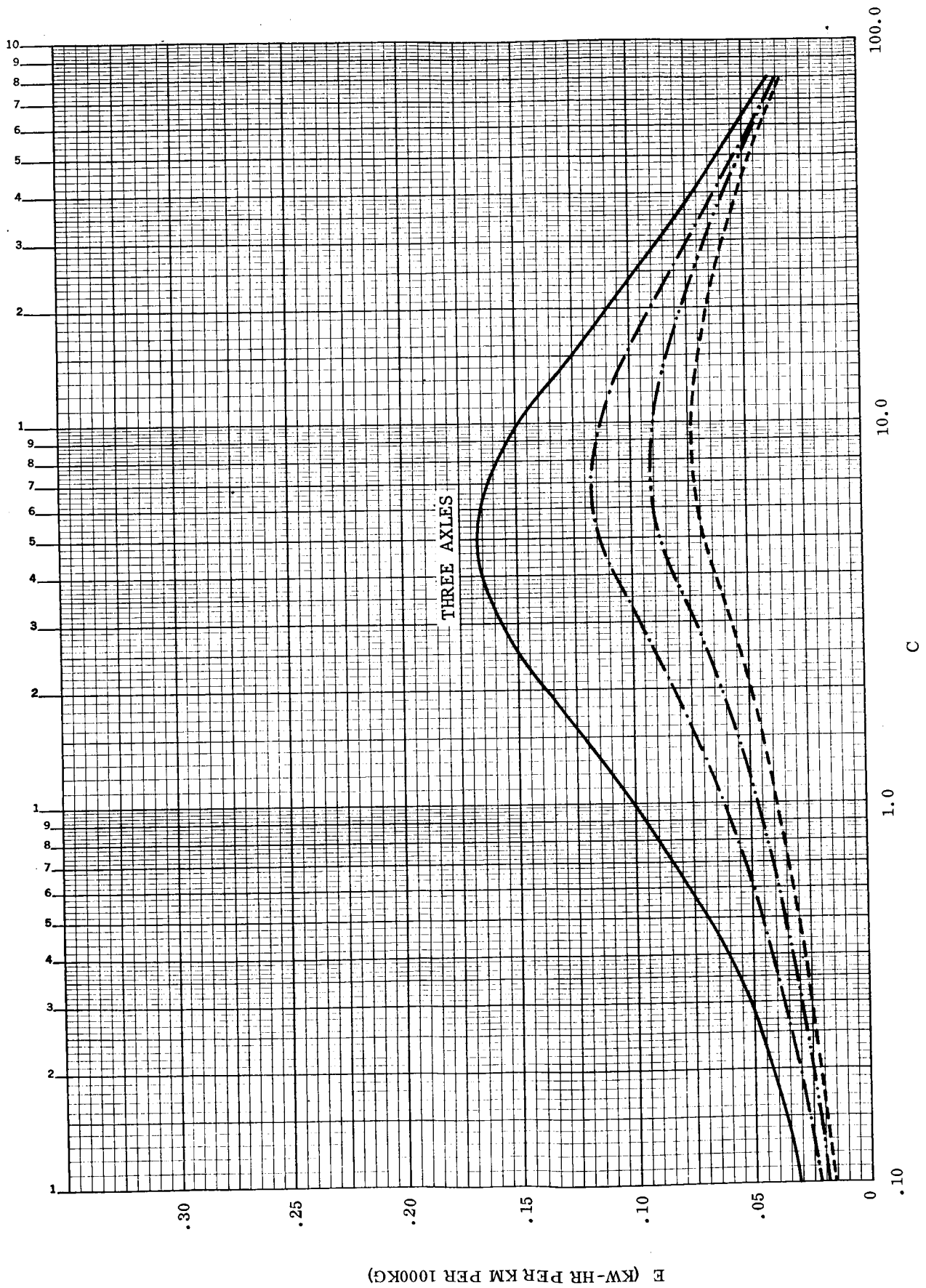


Figure A-8. $DI = 20\text{cm}$, $Y_{\max} = 175\text{cm}$ (Sheet 2 of 2)

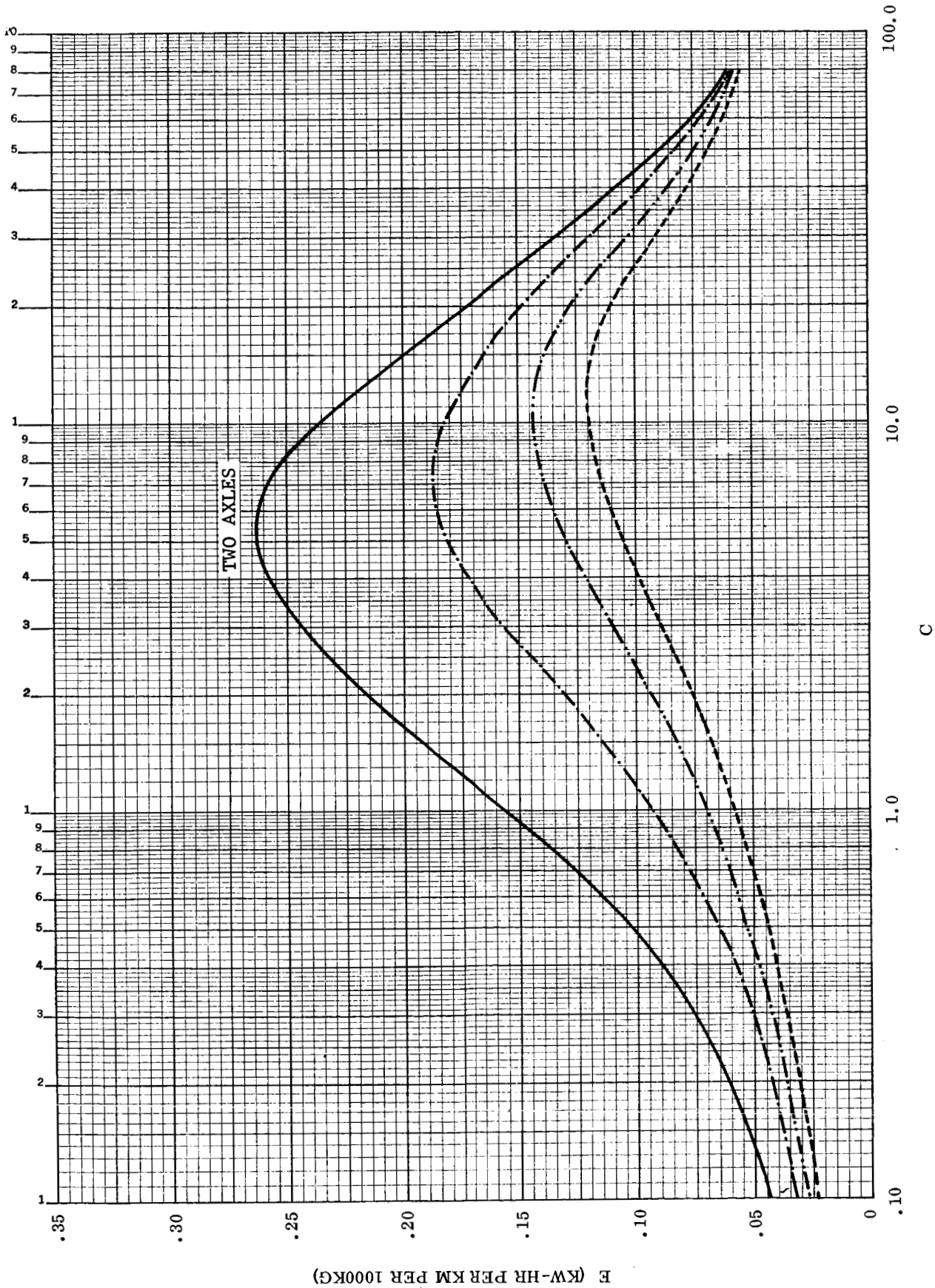


Figure A-9. $DI = 20\text{cm}$, $Y_{\max} = 250\text{cm}$ (Sheet 1 of 2)

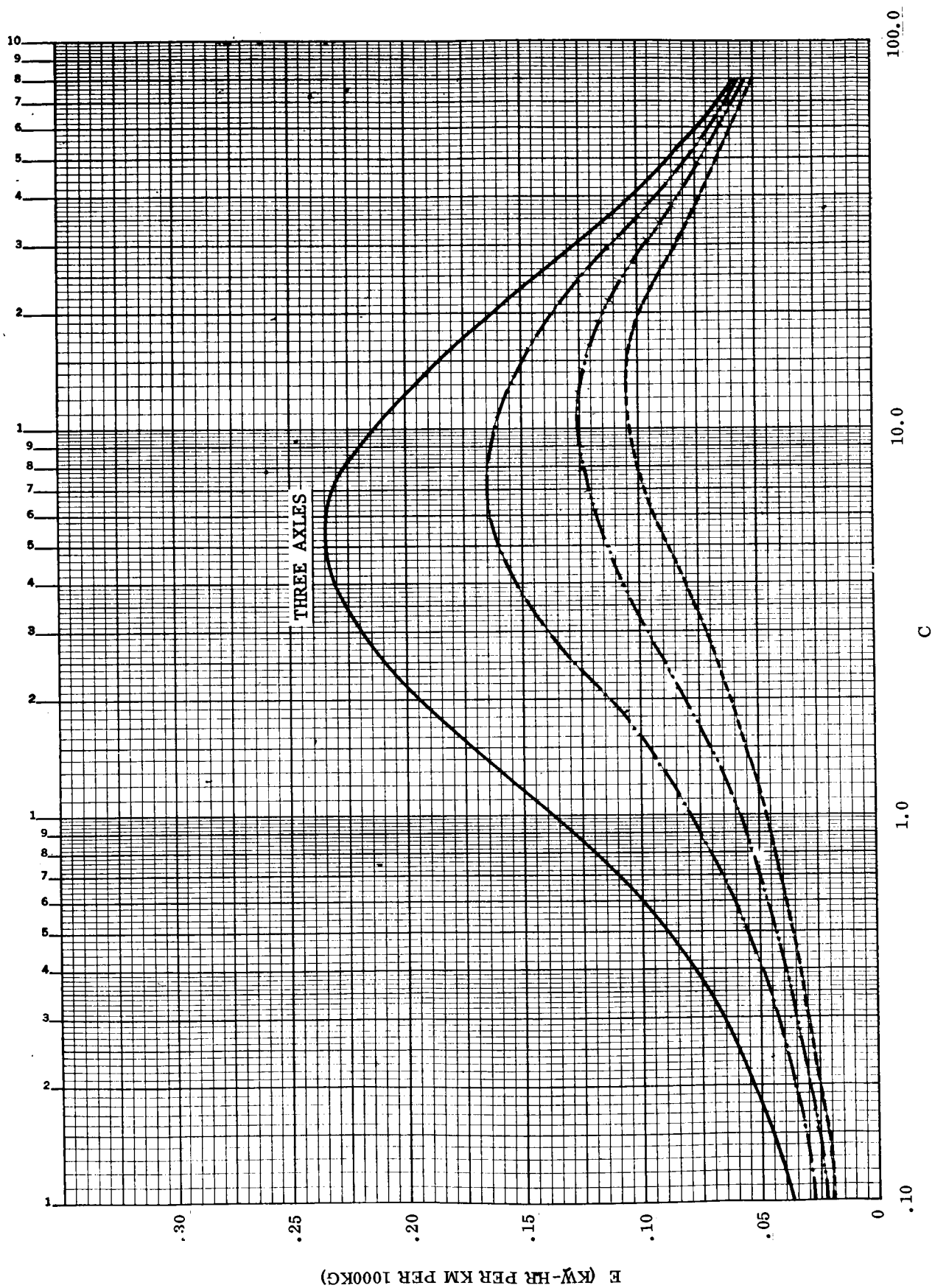


Figure A-9. DI = 20cm, $Y_{max} = 250\text{cm}$ (Sheet 2 of 2)

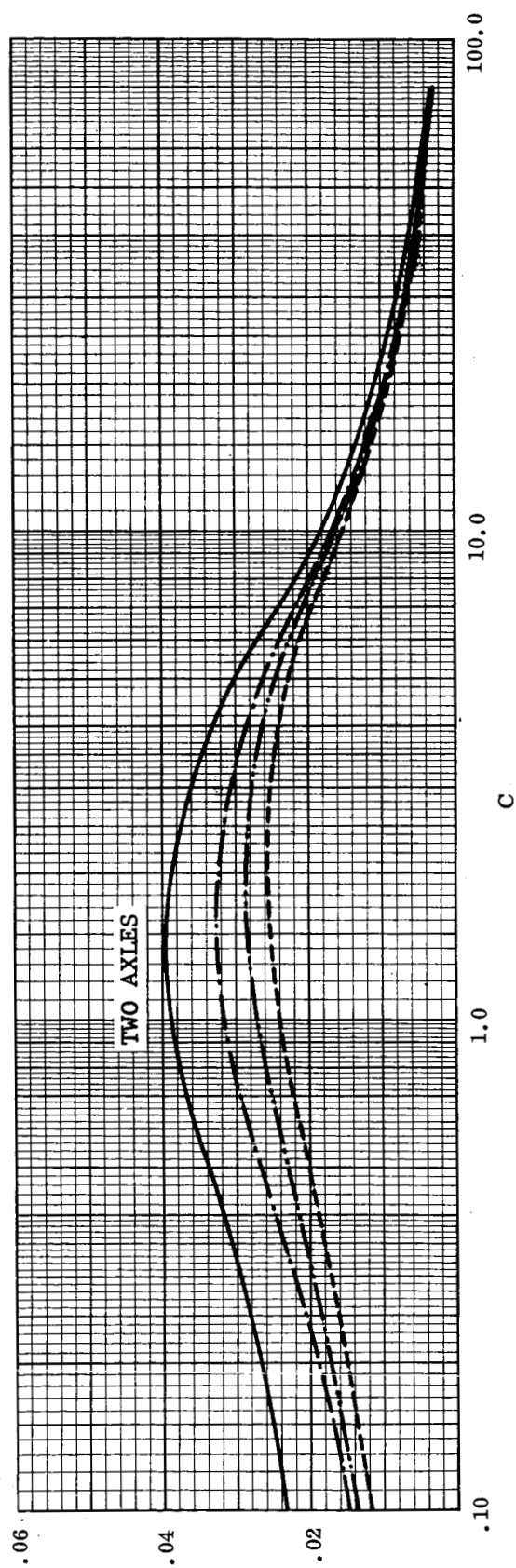
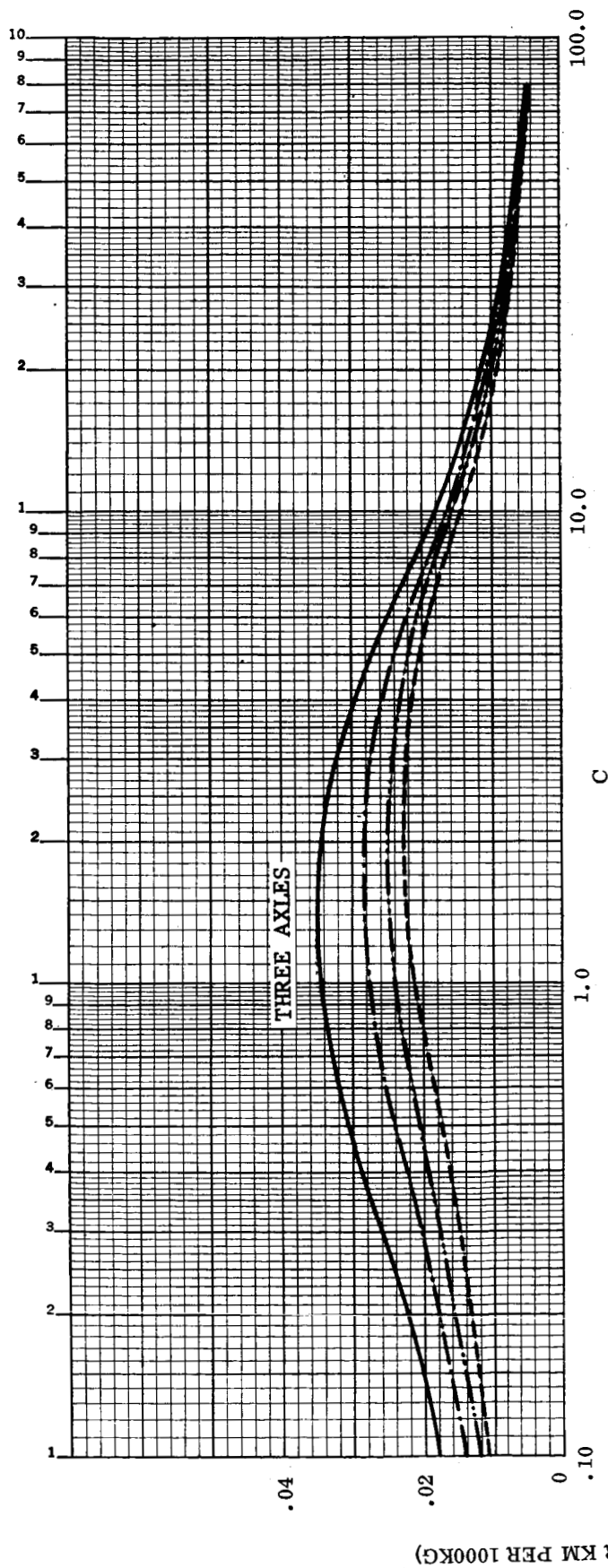


Figure A-10. DI = 40cm, $Y_{max} = 25\text{cm}$

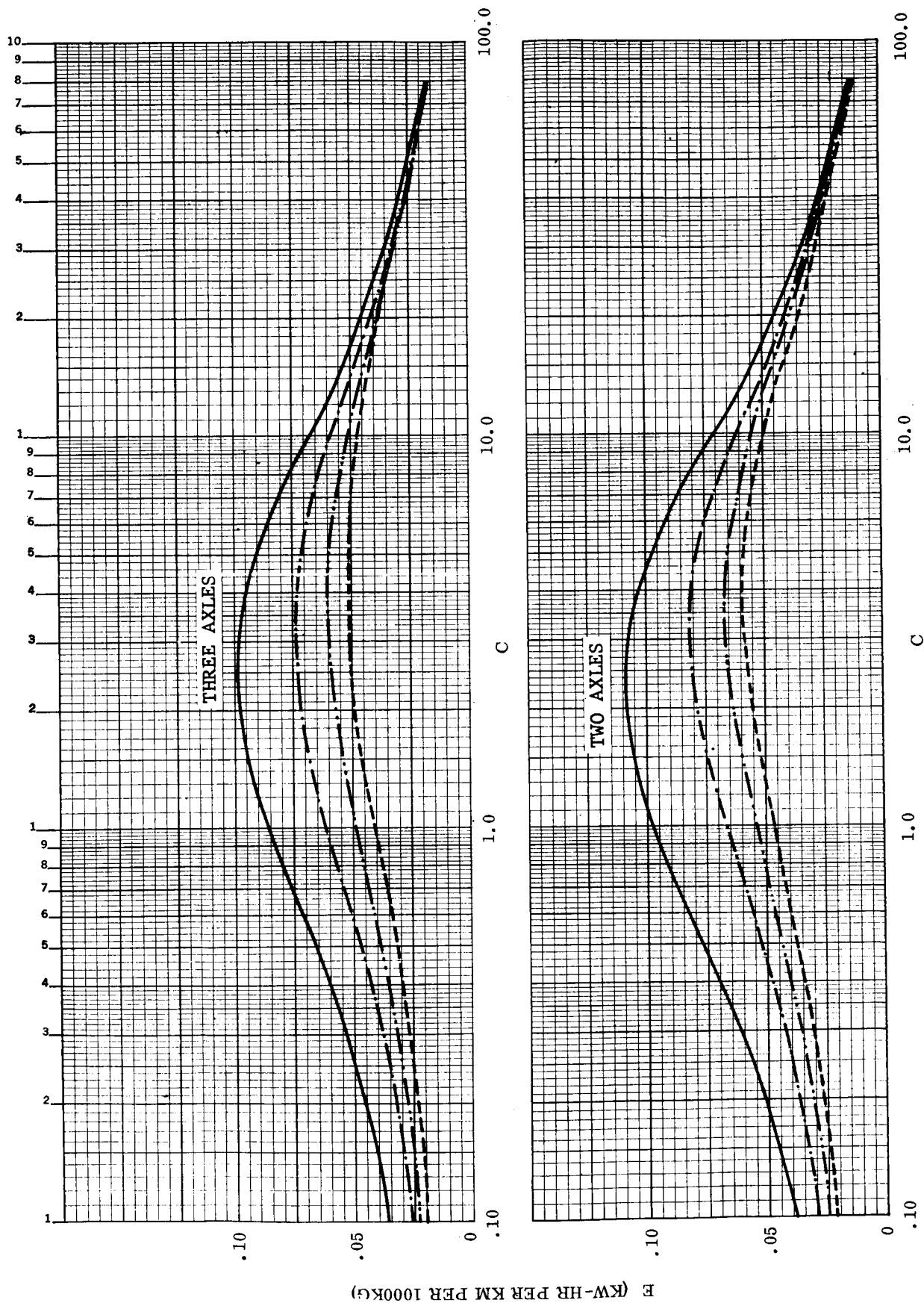


Figure A-11. $DI = 40\text{cm}$, $Y_{max} = 100\text{cm}$

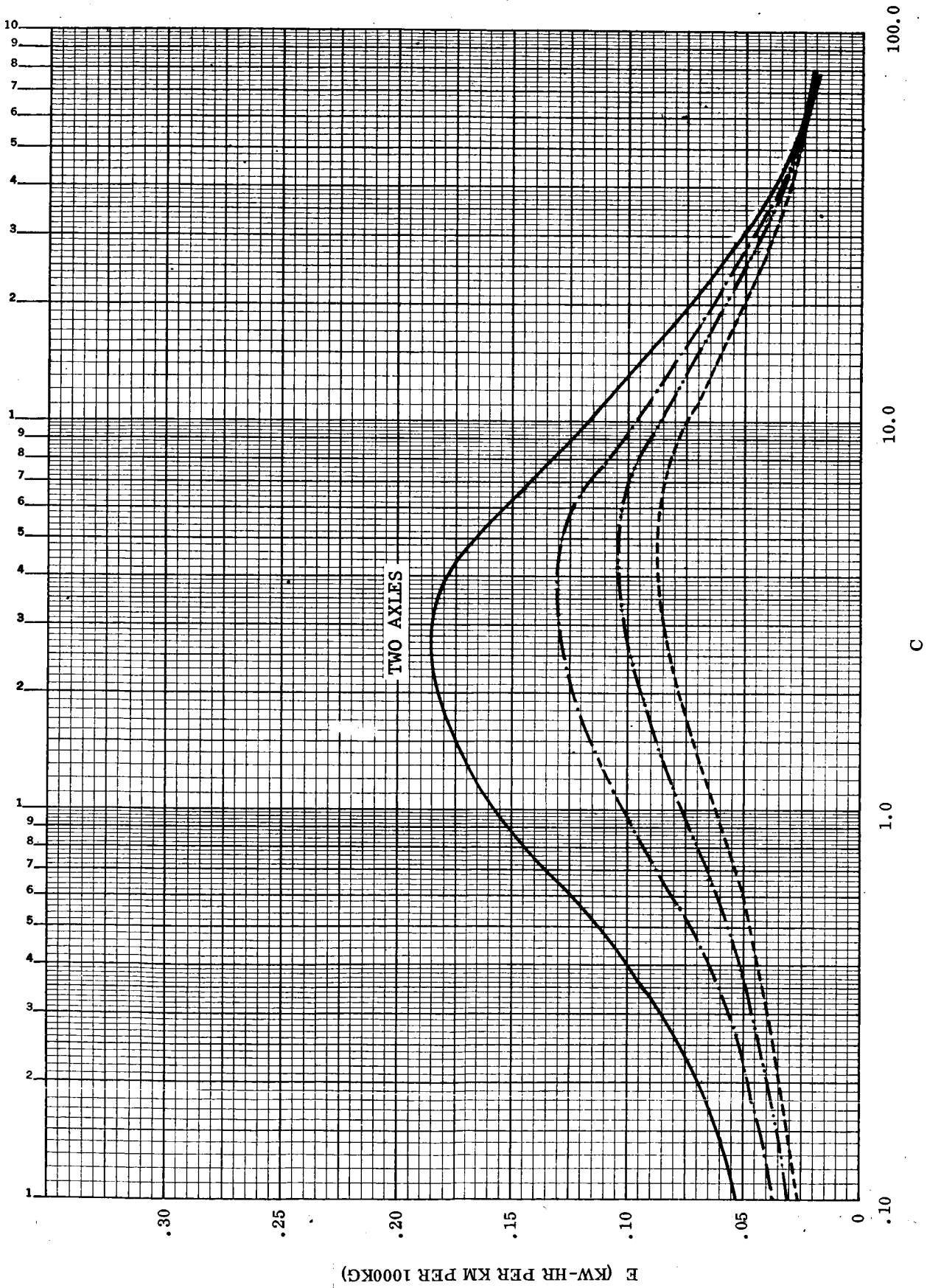


Figure A-12. $DI = 40\text{cm}$, $Y_{\max} = 175\text{cm}$ (Sheet 1 of 2)

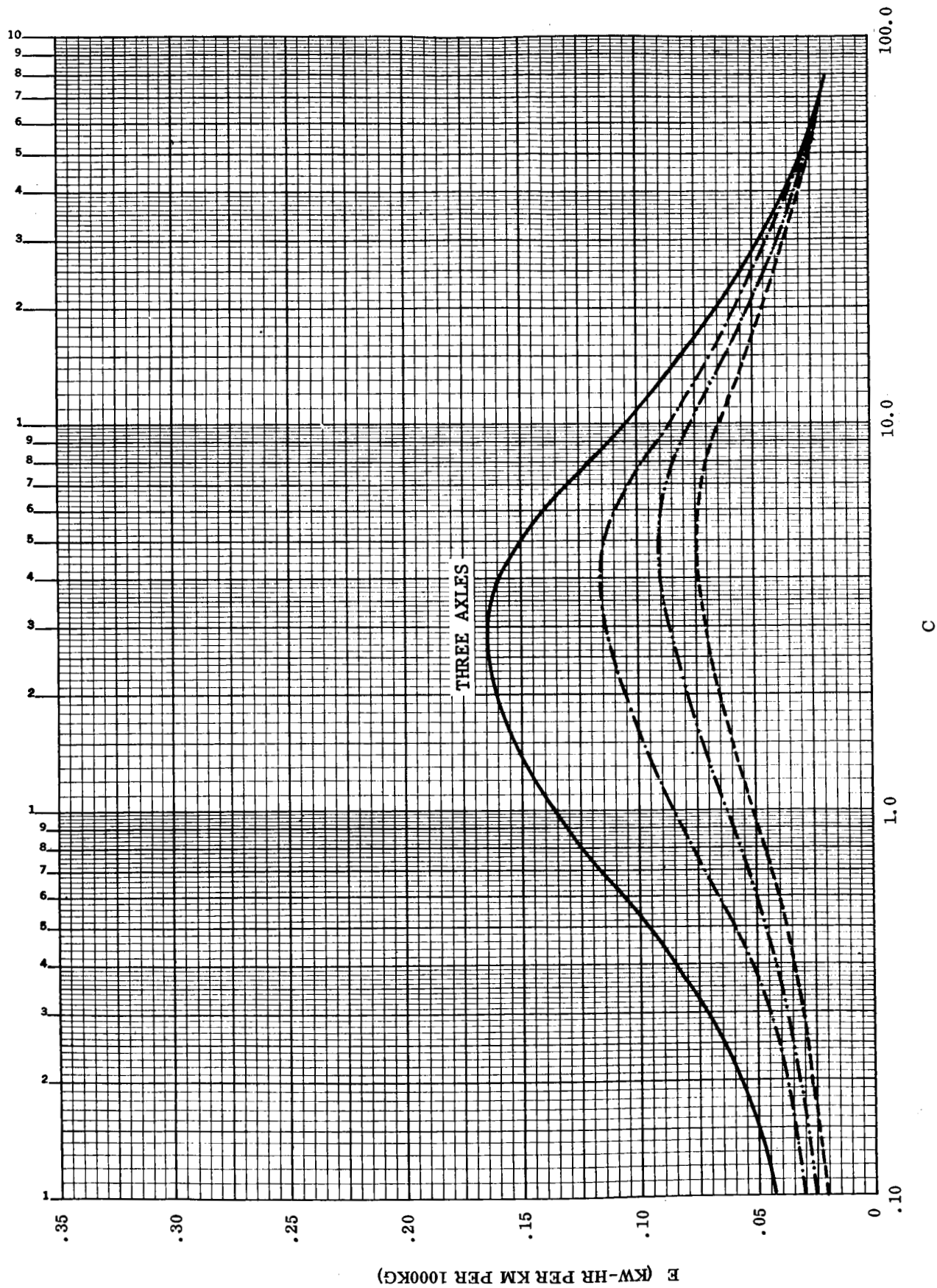


Figure A-12. $DI = 40\text{cm}$, $Y_{\max} = 175\text{cm}$ (Sheet 2 of 2)

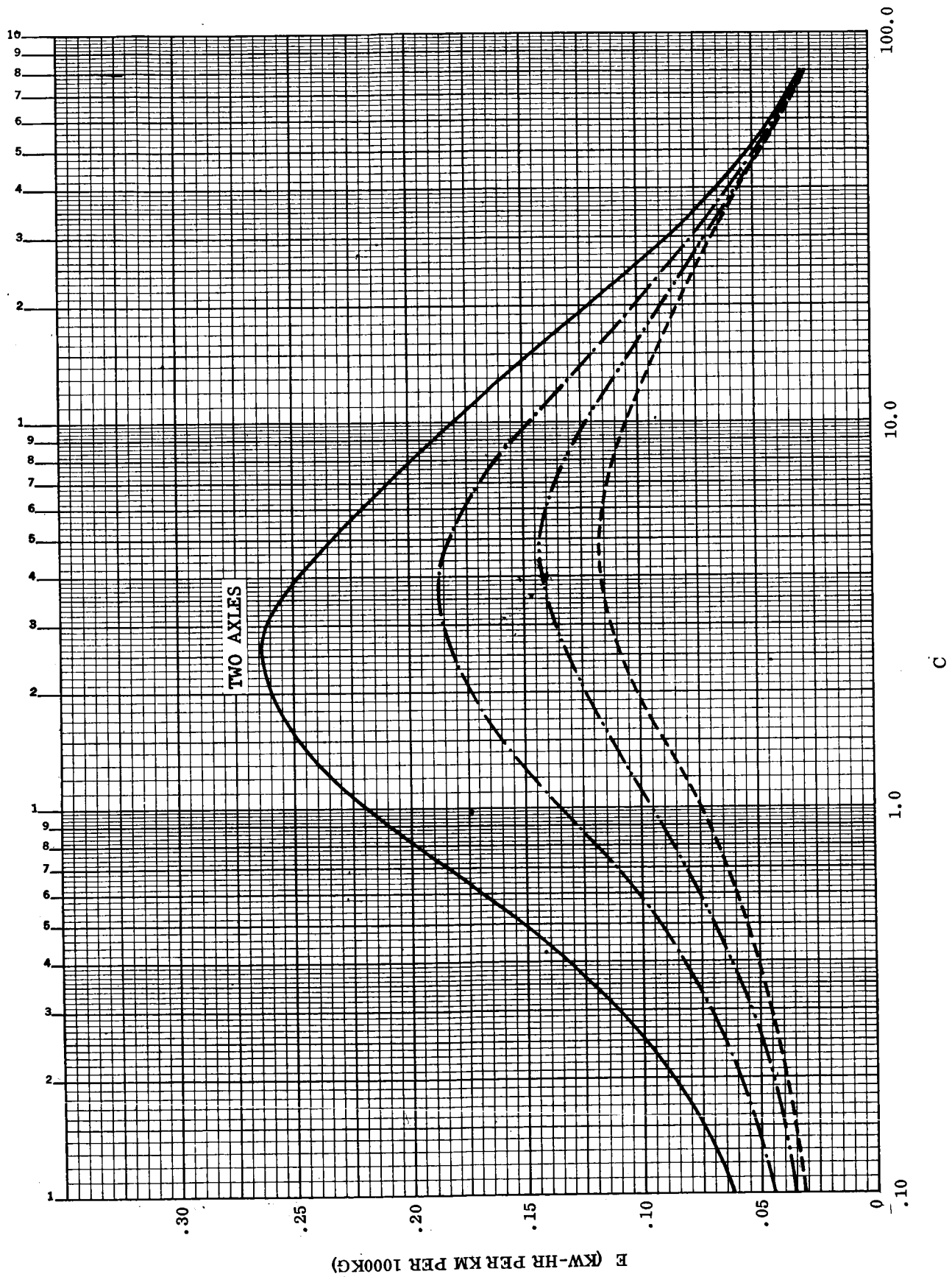


Figure A-13. $DI = 40\text{cm}$, $Y_{\text{max}} = 250\text{cm}$ (Sheet 1 of 2)

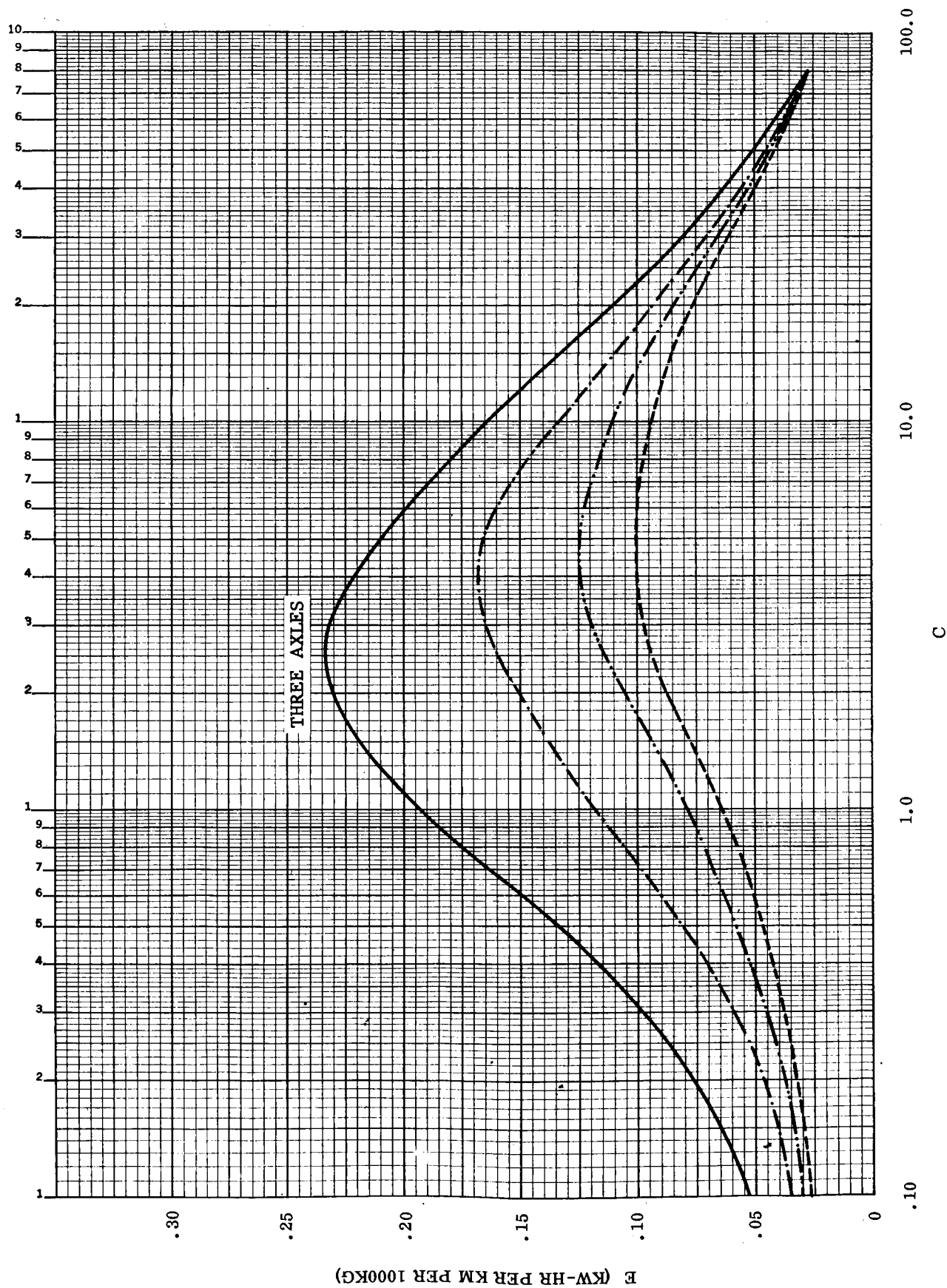


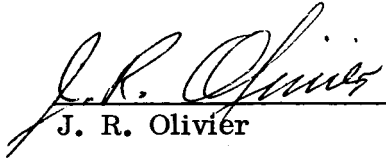
Figure A-13. $DI = 40\text{cm}$, $Y_{\max} = 250\text{cm}$ (Sheet 2 of 2)

APPROVAL

TR-145-D

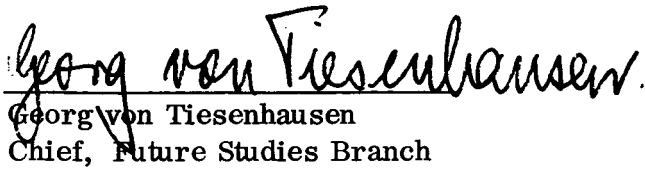
ENGINEERING LUNAR MODEL OBSTACLES (ELMO)

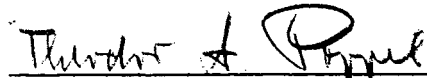
ORIGINATORS:


J. R. Olivier


R. E. Valentine

APPROVALS:


Georg von Tiesenhausen
Chief, Future Studies Branch


Theodor A. Poppel
Director, Launch Support
Equipment Engineering
Division

DISTRIBUTION

Mr. Gray, MT	Mr. Ellsworth, R-P&VE-AA
Mr. Taylor, MT-1	Mr. Perry, R-P&VE-AAO
Mr. Lord, MT-2	Mr. Rains, R-P&VE-AB (5)
Maj. Andrews, MTF	Mr. Laue, R-P&VE-AB
Maj. Evans, MTF	Mr. Love, R-P&VE-AB (5)
Mr. Raffensperger, MTE	Mr. Thompson, R-P&VE-ABO
Mr. Rosenbaum, MTE	Mr. Darwin, R-P&VE-ABS
Mr. Cosal, MTG	Mr. Johns, R-P&VE-AL
Dr. Dixon, MTG	Mr. Vaccaro, R-P&VE-AL
	Mr. De Sanctis, R-P&VE-ALP
Mr. Faget, Asst. Dir, for Eng. Devel.	Mr. Jordan, R-P&VE-AN
Mr. Olling, Dir. SSSO (2)	Mr. Blumerich, R-P&VE-SA
Mr. Davidson, Chief Advanced Program Anal. Off.	Mr. Crawford, R-P&VE-SA
	Mr. Bates, R-QUAL-J
Dr. von Braun, M-DIR	Dr. Stuhlinger, R-RP-DIR
Mr. Maus, E-DIR	Mr. Downey III, R-RP-J
	Dr. Hale, R-RP-J
Dr. Geissler, R-AERO-DIR	Mr. Gierow, R-RP-J
Mr. de Fries, R-AERO-S (5)	Mr. Jones, R-RP-J
Mr. Schaeffer, R-AERO-SP (30)	Mr. Bensko, R-RP-T (2)
Mr. Madewell, R-AERO-SO	
Mr. Bradford, R-AERO-SV	Mr. Dannenberg, R-SA
	Dr. Debus, K-DIR
Mr. Haeussermann, R-ASTR-DIR	Mr. Poppel, K-D
Mr. Digesu, R-ASTR-A	Mr. Owens, K-D
Mr. Dungan, R-ASTR-A	Mr. von Tiesenhausen, K-DF
Mr. Pavlick, R-ASTR-A	Mr. Olivier, K-DF (20)
Mr. Neighbors, R-ASTR-A	Mr. Valentine, K-DF (50)
Mr. Thornton, R-ASTR-A	Mr. Deese, K-FS
	Mr. Adcock, K-DS (2)
Mr. Koelle, R-FP-DIR	
Mr. Waggoner, R-FP	Mr. Claybourne, K-P
Mr. Paul, R-FP	Mr. Knothe, K-T
Dr. Gruene, R-LVO-DIR	Mr. Raffaeili, K-PR2
Mr. Cline, R-P&VE-DIR	
Mr. Goerner, R-P&VE-A	Mr. Haass, MT2545
Mr. Barker, R-P&VE-A	Technical Library, K-GA724 (8)
Dr. Krause, R-P&VE-A	
Mr. Swanson, R-P&VE-A	

DISTRIBUTION (Cont.)

Scientific and Technical Information (25)
P.O. Box 5700
Bethesda, Maryland
Attn: NASA Representative (S-AK/RKT)

EXTERNAL

Dr. M. G. Boyce (3)
Department of Mathematics
Vanderbilt University
Nashville, Tennessee

Dr. T. J. Pignani
Department of Mathematics
East Carolina State College
Greenville, North Carolina

Dr. Robert W. Hunt
Department of Mathematics
Southern Illinois University
Carbondale, Illinois

Dr. Charles C. Conley
Department of Mathematics
University of Wisconsin
Madison, Wisconsin

Dr. Mary Payne
Applied Mathematics Subdivision
Research Division
Engineering Department
Republic Aviation Corporation
Farmingdale, Long Island, New York

Mr. Robert Silber
Department of Mathematics
Southern Illinois University
Carbondale, Illinois

Mr. J. W. Hanson
Computation Center
University of North Carolina
Chapel Hill, North Carolina

Dr. Steve Hu
Northrop Corporation
Box 1484
Huntsville, Alabama

Mr. R. K. Squires
Code 640
Goddard Space Flight Center, NASA
Greenbelt, Maryland

Mr. Dave Engels
Space & Information Systems Div.
Dept. 595/720
North American Aviation, Inc.
Downey, California

Dr. Rudolf Hermann
Director
University of Alabama Research Inst.
4701 University Avenue, N.W.
Huntsville, Alabama

Dr. S. H. Lehnigk
Physical Science Laboratory
Army Missile Command - Bldg. 5429
Redstone Arsenal, Alabama

Mr. William A. Mersman, Chief
Electronic Machine Computing Branch
Ames Research Center
Moffett Field, California

Mr. Howard S. London
Bellcomm, Inc.
1100 17th Street, N.W.
Washington 6, D.C.

DISTRIBUTION (Cont.)

Jet Propulsion Laboratory
4800 Oak Grove Drive
Pasadena 3, California

Langley Research Center
Hampton, Virginia

Mr. David Thomas
NASA - Langley Research Center
Space Mechanics Division
Langley Station
Hampton, Virginia

Mr. R. M. Chapman
Lockheed Missile and Space Company
P.O. Box 1103 West Station
Huntsville, Alabama

Dr. M. L. Anthony
Space Flight Technology
Mail No. A-153
The Martin Company
Denver 1, Colorado

Dr. Joseph F. Shea
Apollo Program Manager
Apollo Spacecraft Program Office
Manned Spacecraft Center
Houston, Texas 77058

Mr. George Cherry
Massachusetts Institute of Technology
Cambridge, Massachusetts

Mr. V. L. Luke
Mathematics and Physics Division
Midwest Research Institute
425 Volker Boulevard
Kansas City 10, Missouri

Dr. Ted Guinn
Advanced Space Technology
Engineering Research
Douglas Aircraft Corporation
Santa Monica, California

Stephen J. Kahne
Lt. USAF
Applied Mathematics Branch
Data Sciences Laboratory
Air Force Cambridge Research Lab.
Office of Aerospace Research
Lawrence G. Hanscom Field
Bedford, Massachusetts

Daniel B. Killeen
Computer Laboratory
Norman Mayer Bldg.
Tulane University
New Orleans, Louisiana 70118

Mr. Jerome S. Shipman
Manager, Mission & Mathematical
Analysis Group
Federal Systems Division IBM
6702 Gulf Freeway
Houston 17, Texas

Mr. Yoshihide Kozai
Smithsonian Institution
Astrophysical Observatory
60 Graden Street
Cambridge 38, Massachusetts

Dr. W. A. Shaw
Mechanical Engineering Department
Auburn University
Auburn, Alabama

DISTRIBUTION (Cont.)

Mr. Hans K. Hinz
Research Department
Grumman Aircraft Engineering Corp.
Bethpage, L. I., New York

Dr. I. E. Perlín
Rich Computer Center
Georgia Institute of Technology
Atlanta, Georgia

Dr. Daniel E. Dupree
Project Leader
Department of Mathematics
Northeast Louisiana State College
Monroe, Louisiana

Mr. Ken Kissel
Aeronautical Systems Division
Applied Mathematics Research Branch
Wright-Patterson Air Force Base
Dayton, Ohio

Dr. J. B. Rosser
Department of Mathematics
Cornell University
Ithaca, New York

Dr. Joseph W. Siry
Theory & Analysis Office (547)
Data Systems Division
Goddard Space Flight Center
Greenbelt, Maryland 20771

Dr. R. P. Agnew
Department of Mathematics
Cornell University
Ithaca, New York

Dr. Jurgen Moser
Professor of Mathematics
Graduate School of Arts & Science
New York University
University Heights, Bronx 53, New York

Mr. Clint Pine
Department of Mathematics
Northwestern State College
Natchitoches, Louisiana

Auburn Research Foundation
Auburn University
Auburn, Alabama

Grumman Library
Grumman Aircraft Engineering Corp.
Bethpage, Long Island, New York

Jet Propulsion Laboratory Library
4800 Oak Grove Drive
Pasadena 3, California

Space Flight Library
University of Kentucky
Lexington, Kentucky

University of Kentucky Library
University of Kentucky
Lexington, Kentucky

Mr. William F. Powers
Department of Aerospace Engineering
University of Texas
Austin, Texas

DISTRIBUTION (Cont.)

Keith Krusemark
Senior Engineer Analyst
Room 1167
Aerospace Industrial Park
General Electric Company
Daytona Beach, Florida

Mr. W. J. Orser
Department of Mathematics
Lehigh University
Bethlehem, Pennsylvania

Dr. J. C. Eaves
Department of Mathematics and Astronomy
University of Kentucky
Lexington, Kentucky

Dr. Henry Hermes
Assistant Professor
Division of Applied Mathematics
Brown University
Providence 12, Rhode Island

Dr. Byron D. Tapley
Department of Aerospace Engineering
University of Texas
Austin, Texas